CORTEX 151 (2022) 188–210

Available online at www.sciencedirect.com

ScienceDirect

Journal homepage: www.elsevier.com/locate/cortex

Clinical neuroanatomy

Regional changes of brain structure during progression of idiopathic Parkinson's disease – A longitudinal study using deformation based morphometry

Peter Pieperhoff [a,*,1], Martin Südmeyer [b,c,1], Lars Dinkelbach [b], Christian J. Hartmann [b], Stefano Ferrea [b], Alexia S. Moldovan [b], Martina Minnerop [a], Sandra Diaz-Pier [e], Alfons Schnitzler [b] and Katrin Amunts [a,d]

[a] Institute of Neurosciences and Medicine (INM-1), Research Centre Jülich, Germany
[b] Department of Neurology and Institute of Clinical Neuroscience and Medical Psychology, Medical Faculty, University Hospital Düsseldorf, Heinrich-Heine-University, Düsseldorf, Germany
[c] Department of Neurology, Ernst-von-Bergmann Klinikum, Potsdam, Germany
[d] C. and O. Vogt Institute for Brain Research, Medical Faculty, University Hospital Düsseldorf, Heinrich-Heine-University, Düsseldorf, Germany
[e] Institute for Advanced Simulation, Jülich Supercomputing Centre (JSC), SimLab Neuroscience, JARA, Research Centre Jülich, Germany

ARTICLE INFO

Article history:
Received 26 August 2021
Reviewed 23 November 2021
Revised 4 February 2022
Accepted 12 March 2022
Action editor Brad Dickerson
Published online 28 March 2022

Keywords:
Parkinson's disease
Longitudinal design
Deformation-based morphometry
Magnetic resonance imaging
Cytoarchitectonic maps

ABSTRACT

Idiopathic Parkinson's disease (PD) is a neurodegenerative disorder with a broad spectrum of motor and non-motor symptoms. The neuropathological characteristics of idiopathic PD are the degeneration of dopaminergic neurons in the striatum, and the propagation of aggregates of misfolded α-synuclein in the brain following a specific pattern (Braak et al., 2006). The relationship of this pattern with motor and cognitive symptoms is still equivocal. Therefore, we investigated longitudinally the spatio-temporal patterns of atrophy propagation in PD, their inter-individual variability and associations with clinical symptoms. Magnetic resonance (MR) images of 37 PD patients and 27 controls were acquired at up to 15 time-points per subject, and over observation periods of up to 8.8 years (mean: 3.7 years). MR images were analyzed by Deformation-based Morphometry to measure region volumes and their longitudinal changes. Differences of these regional volume data between patients and controls and their associations with clinical symptoms were calculated.

At baseline, group differences in the regional volumes were found mainly in areas of the sensory, motor and orbitofrontal cortices, areas in the frontal operculum, inferior frontal sulcus, hippocampus and entorhinal cortex, and in the substantia nigra, among others.

* *Corresponding author*. Institute of Neuroscience and Medicine 1 (INM-1), Research Centre Jülich, D-52428 Jülich, Germany.
E-mail address: p.pieperhoff@fz-juelich.de (P. Pieperhoff).
[1] Authors P.P. and M.S. contributed equally to this study.
https://doi.org/10.1016/j.cortex.2022.03.009

The longitudinal analysis yielded more widespread and more pronounced group differences, with significantly accelerated volume decreases in PD patients in the occipital and temporal lobes, the inferior parietal lobule, as well as in the insula, putamen and nucleus basalis Meynert. The white matter was less affected than the gray matter. Worse clinical scores (MMSE, PDQ-39, UPDRS-III) were in particular associated with volume decreases of cortical areas, amygdala and basal forebrain nuclei, but not of the basal ganglia. The observed longitudinal patterns of accelerated volume decrease in PD patients largely coincide with the pattern of α-synuclein pathology in PD stages 3–5 as proposed by Braak and colleagues. Thus, longitudinal DBM appears to depict already in-vivo the progression of neuropathological changes.

1. Introduction

Neuropathological hallmarks of idiopathic Parkinson's disease (PD) are the degeneration of dopaminergic neurons and the occurrence of Lewy-bodies (LB) and -neurites (LN) which were first described by Lewy (Forno, 1996; Lewy, 1912): These intraneuronal inclusions consist mainly of aggregates of misfolded α-synuclein (αSyn) (Polymeropoulos et al., 1997; Spillantini et al., 1997). The distribution pattern of LB/LN in the brain was examined by Braak and colleagues in 168 post-mortem brains using αSyn-staining (Braak et al., 2003). They postulated therefrom a six-stage scheme for the progressive propagation of the αSyn pathology in PD: Beginning in the lower brain stem nuclei and olfactory bulb (stage 1), the pathology raises through the nuclei of the pontine tegmentum (stage 2), until it reaches the midbrain and in particular the substantia nigra (stage 3). From there it passes through the temporal mesocortex and allocortex (stage 4) to sensory association areas, prefrontal cortex, and finally to the premotor cortex and primary sensory and motor cortices (stages 5, 6) (Braak et al., 2003). This scheme was challenged by another neuropathological study (Parkkinen, Kauppinen, Pirttilä, Autere, & Alafuzoff, 2005; Parkkinen, Pirttilä, & Alafuzoff, 2008), which reported that about 50% of subjects with severe αSyn-pathology (Braak PD stages 5, 6), had not suffered from extrapyramidal motor symptoms (EPS) or dementia.

In-vivo markers of PD-related neurodegeneration could improve the understanding of the functional impairments in PD, while methods for directly imaging aggregated αSyn are still lacking (Brooks & Tambasco, 2016). The density of dopamine receptors can be mapped by appropriate PET and SPECT tracers, but its relationship with the loss of dopaminergic neurons is not straightforward, because in the early phases of PD their density could be even up-regulated, followed by a down-regulation in later phases (Kaasinen, Vahlberg, Stoessl, Strafella, & Antonini, 2021). Structural magnetic resonance (MR) imaging is used in PD research mainly to characterize local brain structure by e.g., volumetric measures, cortical thickness, or gray and white matter (GM, WM) "density" maps (voxel-based morphometry (Burton, McKeith, Burn, Williams, & O'Brien, 2004)), but also to estimate local tissue properties such as fiber integrity, or the deposition of iron and melanin.

Neuroimaging studies of brain structure using a cross-sectional design reported volume reductions in PD patients' brains in the putamen, and in the temporal, occipital and parietal lobes (Beyer, Janvin, Larsen, & Aarsland, 2007; Borroni et al., 2015; Burton et al., 2004; Duncan et al., 2016; Lee et al., 2014; Pereira et al., 2012; Summerfield et al., 2005). These reductions were most pronounced in brains of PD patients with cognitive impairments or longer disease duration, whereas comparisons of early-stage patients with healthy controls sometimes even failed to demonstrate volumetric differences (Borroni et al., 2015; Menke et al., 2014; Planetta et al., 2015). A comprehensive study of 232 PD patients and 117 controls using Deformation-Based Morphometry indicated atrophy in the midbrain, basal ganglia, basal forebrain and medial temporal lobe in early disease stages (Zeighami et al., 2015, 2019).

Longitudinal studies are necessary to investigate the dynamics of structural changes and to distinguish them from those that occur during healthy aging. Using a longitudinal design, differences in brain size changes between controls and demented PD patients have been found, while controls and cognitively normal PD patients did not differ (Burton, McKeith, Burn, & O'Brien, 2005). Progressive volume declines in demented and non-demented PD patients were reported, with accelerated volume declines in hippocampus, insula, occipital and temporal lobes and in the cingulate gyrus (Gee et al., 2017; Ramírez-Ruiz et al., 2005). The later studies, however, did not examine controls. An accelerated expansion of the ventricles in early-stage patients also had been observed (Lewis et al., 2009). In several studies, subjects were observed over periods between one and three years, and the subjects were examined at two or three time-points (Gee et al., 2017). A common pattern of these studies was that the atrophy rates were particularly increased in PD patients with dementia in comparison with non-demented patients or controls, whereas only little evidence was found for an association between changes of motor impairments and structural changes (Lewis et al., 2009). Recent investigations of cortical thickness (Filippi et al., 2020; Gorges et al., 2020; Mak et al., 2015) of PD patients and controls found differences which were related with cognitive impairments.

The present study evaluated differences between PD patients and controls in regional volumes at baseline (i.e., each subject's first time point) and their longitudinal changes over

Table 1 – Distribution of age and clinical scores at the baseline examination and last examination, number of examinations and observation periods of patients and controls of the samples which were used for the baseline and longitudinal analyses. The mean examination interval is the average interval between consecutive examinations. Clinical scores are explained in the text. For each parameter the mean value, standard deviation, minimum and maximum are listed. LEDD = levodopa equivalent daily dose [mg].

	PD patients	Controls
Baseline sample		
Number	50	50
Male/female	33/17	33/17
Age [years]	55.1 ± 12.1 (34.6–77.7)	56.9 ± 12.5 (29.3–78.5)
Disease duration [years]	3.9 ± 3.1 (.4–9.2)	–
UPDRS-III	15.4 ± 11.2 (1–45)	–
MMSE	28.5 ± 2.1 (24–30)	29.0 ± 1.6 (25–30)
PDQ-39	23.1 ± 20.1 (0–76)	–
Hoehn–Yahr	1.8 ± .7	–
Longitudinal sample		
Number	37	27
Male/female	24/13	12/15
Initial age [years]	53.2 ± 12.9 (32.6–74.4)	60.7 ± 10.3 (35.5–75.5)
Last age [years]	57.2 ± 12.5 (33.2–77.9)	64.0 ± 10.1 (39.1–82.6)
Initial disease duration [years]	3.7 ± 2.3 (.4–9.2)	–
Last disease duration [years]	7.9 ± 2.3 (2.5–12.2)	
Initial UPDRS-III	15.5 ± 11.1 (1–45)	–
Last UPDRS-III	23.8 ± 8.8 (8–43)	–
Initial MMSE	28.6 ± 2.1 (24–30)	28.8 ± 1.6 (25–30)
Last MMSE	27.9 ± 3.1 (14–30)	29.5 ± .7 (28–30)
Initial PDQ-39	19.2 ± 19.6 (0–76)	–
Last PDQ-39	33.8 ± 30.4 (0–103)	–
Initial Hoehn–Yahr	1.7 ± .7	–
Initial LEDD [mg]	493 ± 562 (0–2520)	–
Last LEDD [mg]	730 ± 402 (98–1680)	–
Number of time points per subject	8.1 ± 3.6 (2–15)	4.2 ± 1.5 (2–7)
Observation period [years]	3.9 ± 2.3 (.6–8.8)	3.3 ± 2.5 (.9–7.9)
Mean examination interval [years]	.56 ± .32 (.15–2.91)	1.05 ± .89 (.22–5.48)

periods of up to 8.8 years The spatial patterns, by which regional volume changes occurred, were characterized by using cytoarchitectonic maps, which had been derived from postmortem analysis. Furthermore, we analyzed in the patients group the associations of these regional volume data to motor symptoms, cognitive status and a quality-of-life score.

2. Materials and methods

2.1. Subjects

Fifty PD patients and fifty controls were examined at baseline. Longitudinal data had been acquired of 37 PD patients and 27 healthy controls. Patients were asked for participation during stays for diagnostic clarification or evaluation of therapeutic options on the specialized ward for movement disorders. Inclusion criteria of patients were a diagnosis according to UK Parkison's Disease Society Brain Bank criteria (see below), age above 18 years, and absence of any neurological or psychiatric disorder apart from PD. Nuclear medicine examinations were available of 27 patients, i.e., 73 % of the longitudinal sample, and 54% of the cross-sectional sample. Controls were recruited among spouses of patients, hospital staff and via advertisements. Exclusion criteria for controls were active or past neurological or psychiatric diseases. These inclusion/exclusion criteria had been determined before starting this study. Data of patients and controls had been acquired over several years. Therefore, the final size of the sample and the observation period of each participant could not be predetermined in advance. This study was performed in accordance to the declaration of Helsinki and approved by the local Ethics committee (N: 2849). All participants provided written informed consent.

The demographical and clinical baseline data are listed in Table 1. The disease duration of patients at baseline ranged from .4 to 9.2 years (mean 3.9 ± 2.3 years). Patients were examined up to 15 times over a maximum period of 8.8 years. The mean interval between examinations was .56 years, resulting in a total amount of 298 measurements. Controls were examined up to 7 times over a maximum period of 7.9 years (mean interval: 1.05 years), summing up to 113 measurements.

2.2. Clinical examinations

Diagnosis of idiopathic PD was made according to UK Parkinson's Disease Society Brain Bank clinical diagnostic criteria. Assessments were conducted in the ON-state under regular patient-medication. They always took place in the late afternoon. Motor impairments were assessed by the Unified Parkinson's Disease Rating Scale – Section III (UPDRS-III) (Goetz et al., 2008), and cognitive state by the "Mini-mental state examination" (MMSE) (Folstein, Folstein, & McHugh, 1975). In the PD patients group, the impact of PD on individual health status and health-related quality of life was evaluated by the PDQ-39 questionnaire (Peto, Jenkinson, Fitzpatrick, & Greenhall, 1995).

2.3. Image acquisition and analysis

T1-weighted MR images were acquired either on a Siemens Magnetom Vision 1.5 T, or on a Magnetom Trio Tim 3.0 T scanner (Siemens Medical Solutions, Erlangen, Germany). A 3D gradient echo sequence with isotropic voxel size 1 mm was utilized (1.5 T scans: TR 9.7 msec, TE 4.0 msec. 3.0 T scans: TR 2300 msec, TE 2.98 msec). Each subject's series of MR images was acquired on one and the same scanner and with the same MR sequence to avoid variations in the MR images of a given series due to technical causes. The MR images were visually checked for disturbances (in particular movement artefacts) immediately after their acquisition, so that the acquisition could be repeated, when necessary. Every MR image was again

visually checked for disturbances before it was included in the analysis. These criteria are usual practice for morphometrical studies, and were determined in advance, based on the experience of previous studies. In the longitudinal sample MR images of 22 of 433 time points had to be discarded (21 of patients, one of controls), most of them because of movement artefacts. In the baseline sample two MR image acquistions had to be repeated.

The images were analyzed by Deformation-Based Morphometry (DBM), which enables the calculation of volumetric differences of brains based on the non-linear registration of their 3D MR images (Pieperhoff et al., 2008).

2.3.1. Baseline analysis

All baseline MR images were registered with the MNI single subject T1 reference template ("Colin27") (Holmes et al., 1998): Therefore, the MR images were segmented using SPM12 (Ashburner & Friston, 2005), which yielded masks of gray and white matter. These were merged into binary masks of each brain, which were visually checked and corrected, when necessary, by using the program itk-SNAP (Yushkevich et al., 2006). Intensity inhomogeneities were corrected by the program N4 (Tustison et al., 2010). The segmented images were affinely registered with the reference image by using the program FSL-flirt (Jenkinson & Smith, 2001), followed by a symmetrical non-linear registration: The MR images were locally deformed, such that a similarity measure (cross correlation) was maximized, under the constraint of a regularizer, which modeled an elastic deformation. The regularizer was applied to avoid strong distortions which were not biologically meaningful (Henn, 2003; Modersitzki, 2003). Maps of "local volume ratios" ($\mathrm{LVR}(\vec{x})$) were derived from the deformation fields, which specify for each voxel of the reference brain the volume of the corresponding volume element in the brain of a given subject (Fig. 1A–F). This enables to calculate in each subject's brain the volumes of anatomical regions. Regions are defined in the reference brain by atlases which contain probabilistic maps and regional label maps (see below). Region volumes of each subject were calculated by the following formula, which sums the LVR values over the voxels in the reference brain:

$$V_{Region} = \sum_{\vec{x} \in \Omega_{Region}} \mathrm{LVR}(\vec{x}) \cdot p_{Region}(\vec{x}) \cdot V_{voxel}$$

In a probabilistic map $p_{Region}(\vec{x})$ is the probability that voxel $\vec{x}$ of the reference brain belongs to the considered region, whereas in a label map $p_{Region}(\vec{x})$ is an indicator function, which is equal to one when $\vec{x}$ is inside a given region, and zero outside. V_{voxel} is the volume of a voxel (1 mm^3). The deformation fields were also used to transform the brain atlases from the reference space into the baseline MR image of each subject for the calculation of longitudinal regional volume changes (Fig. 1G).

The intracranial volume (ICV), which was used as a covariate in the baseline analyses, was measured by its manual segmentation in every tenth sagittal section of an MR image, beginning in the midsagittal section, and linear interpolation of interjacent sections.

2.3.2. Longitudinal analysis

For the analysis of longitudinal regional volume changes the follow-up images of a given subject were symmetrically registered with its baseline MR image (Fig. 1H, I), so that an LVR-map was calculated for each subject and each follow-up time point (Fig. 1L, M). Most of the applied procedures were the same as for the baseline analysis, but the images were not segmented for the registration. In addition, a symmetric registration was calculated, i.e., both, the baseline and the follow-up image were deformed until they were matched, and the similarity metric (cross-correlation) was calculated in a local neighborhood of each voxel. The later approach was chosen because this metric had been shown to be less sensitive to intensity inhomogeneity artefacts of the MR acquisition than metrics which are globally evaluated, i.e., over the complete image (Studholme, Drapaca, Iordanova, & Cardenas, 2006).

Then, for each time point, the regional volume relative to the baseline volume (i.e., the fraction of the baseline volume) was calculated for each subject as follows:

$$v_{Region}(t) = \frac{V_{Region}(t)}{V_{Region}(0)} = \frac{\sum_{\vec{x} \in \Omega_{Region}} \mathrm{LVR}(t, \vec{x}) \cdot p_{Region}(\vec{x})}{V_{Region}(0)} \cdot V_{voxel}$$

$V_{Region}(0)$ is the baseline volume of a given region in the brain of a subject, and $p_{Region}(\vec{x})$ is the probability (or indicator) function of the region in the subject's baseline image. The later results from the transformation of the brain atlases into each subject's baseline image. Relative volumes were analyzed instead of differences in absolute volumes because interindividual differences of the later are generally much larger than individual volume changes, and thus complicate their analysis.

2.4. Brain atlases

The voxel-wise LVR-data, which result from the DBM-analysis, were spatially averaged over the atlas regions to yield estimates of regional volume data (or their changes), because these data are more robust than voxel-wise estimates. Moreover, region-based data can be directly compared between different subjects or groups, and thus facilitate their statistical analysis and interpretability. The following atlases and segmentations of the Colin27-brain were used:

(a) The Julich-Brain Atlas (Amunts, Mohlberg, Bludau, & Zilles, 2020; Amunts & Zilles, 2015) is based on the cytoarchitectonic mapping of cortical areas and subcortical nuclei in ten post-mortem brains. It provides a parcellation of the brain based on its microstructure. The individual maps were transformed into a common reference space to yield probabilistic maps which reflect their inter-individual spatial variability (see Supplemental Table 2).

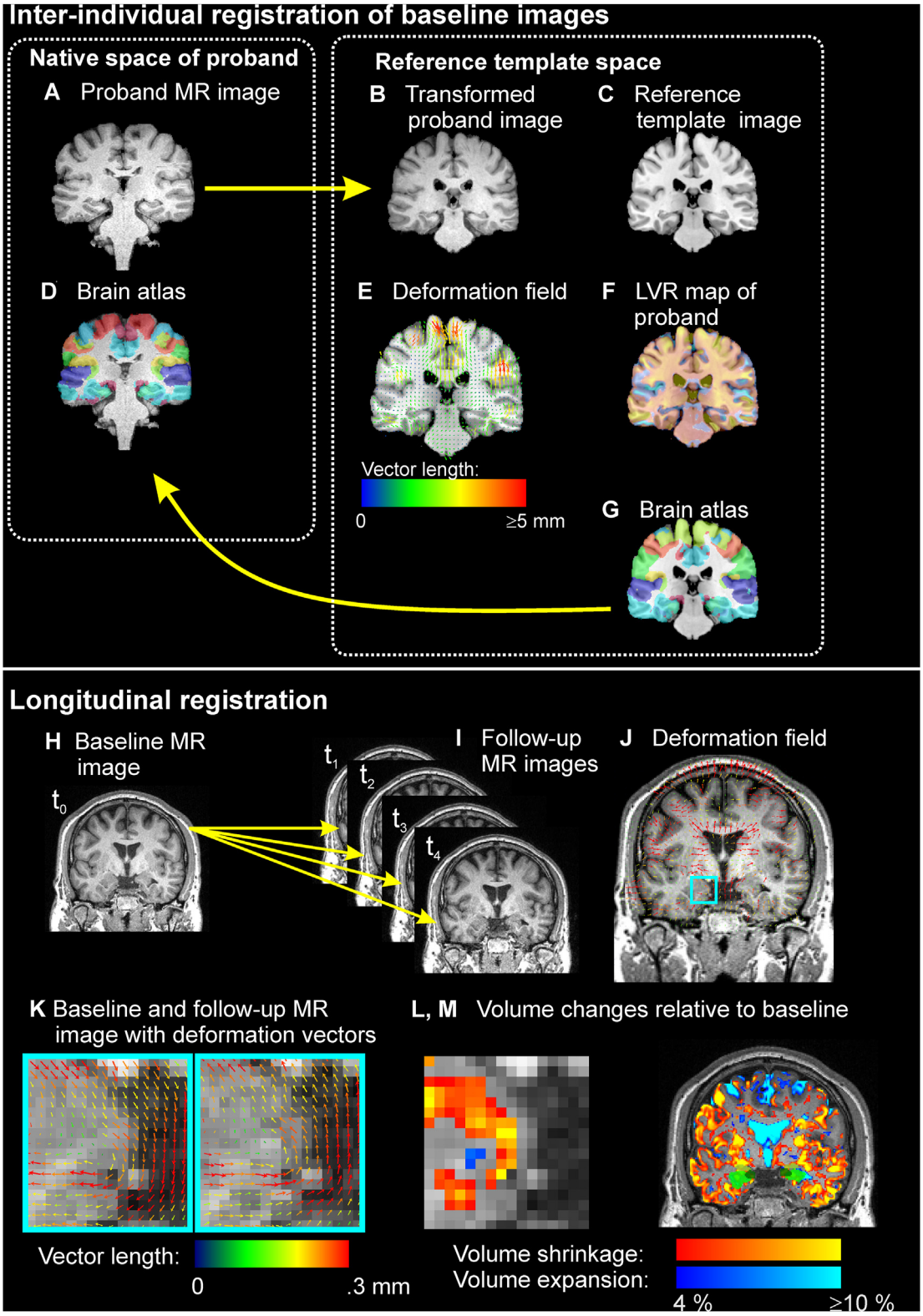

Fig. 1 – Image analysis methods to detect volume differences and longitudinal changes. MR-images were analyzed by deformation-based morphometry to detect differences between groups in region volumes at baseline, and in their longitudinal changes. (A–G) Cross-sectional analysis of baseline images. (A) Each MR (source image) images is segmented, such that only the brain tissue remains in the image. The segmented images is registered with a reference template image. (B) Transformed MR image, (C) Reference template image, onto wich the image in (B) is transformed. (D) Deformation field, i.e., a vector field, which encoded the non-linear transformation. The color indicates the vector length (E) LVR-map, i.e., map of voxel-wise volume differences between the reference template and the source image. (F) Brain atlas in the space of the

(b) The AAL3 atlas (Rolls, Huang, Lin, Feng, & Joliot, 2020; Tzourio-Mazoyer et al., 2002) (https://www.gin.cnrs.fr/en/tools/aal/), contains regional labels of the Colin27 brain. Region maps of subcortical nuclei (basal ganglia, nucleus accumbens, thalamus, brainstem nuclei) and cerebellar lobules, which are not yet covered by the Julich-Brain atlas, where used in this study (see Supplemental Table 3).
(c) Maps of the global gray and white matter of the Colin27 brain (Aubert-Broche, Evans, & Collins, 2006) (http://nist.mni.mcgill.ca/?p=947).
(d) Maps of the complete hemispheres and ventricles of the Colin27 brain.

2.5. Statistical analysis

2.5.1. Baseline analysis

Cross-sectional differences between patients and controls in the baseline regional volumes were analyzed for each region separately by an ANCOVA model: The dependent variable was the region volume, and predictor variables were group, sex, age, intracranial volume (ICV), and the interaction age × group. Two-tailed t-tests were applied to test whether the group difference was significantly different from zero at the level $p \leq 0.05$ (uncorrected for multiple comparisons, see below).

Pearson correlations were calculated between the residuals of the regional volumes of the previous ANCOVA and each of the parameters UPDRS-III, MMSE and PDQ-39. Only data of the patients were used for this analysis. The residuals of the volume data were analyzed instead of the region volumes because the former were adjusted for the covariates age, icv and sex.

2.5.2. Longitudinal analysis

The longitudinal data of this study were examined by uni- and bivariate linear mixed models (LMM) (Verbeke & Molenberghs, 2000). These models are widely used for longitudinal analyses, because they are capable to account appropriately for differences among subjects in the number of measurements or their time-points Δt (i.e., the time difference to the baseline measurement). An LMM is an advanced regression model, which takes into account that the measurements of a given subject are correlated with each other. All available data of all subjects are simultaneously analyzed by a restricted maximum likelihood approach (Verbeke & Molenberghs, 2000).

Models that included the clinical parameters were again based on the PD patients' data only. Relative region volume changes were included by their logarithms in order to make their distribution more symmetric (Leow et al., 2007). Two-tailed t-tests were applied to test whether single model parameters were significantly different from zero. The following statistical models were analyzed:

- Time-dependent changes of each clinical score (UPDRS-III, PDQ-39, MMSE) were examined by a univariate LMM. The only predictor was Δt. Its fixed effect was tested.
- Group differences of the longitudinal relative volume data were examined by a univariate LMM. Predictors were Δt and the interactions of Δt with each subject's group ($\Delta t \times group$), sex ($\Delta t \times sex$), and baseline age ($\Delta t \times age_0$). The later accounted for age-related changes in atrophy rates. It was tested whether the regression coefficient of $\Delta t \times group$ was significantly different from zero, i.e., whether there was a group difference in the relative volume change rates. Note that the logarithms of relative volume changes are by definition zero at baseline ($t = 0$), therefore main effects of group or sex are not part of these models, but only their interactions with time.
- Associations between change rates of relative region volumes and each of the clinical variables were examined by a bivariate LMM (Thiébaut, Jacqmin-Gadda, Chêne, Leport, & Commenges, 2002): Response variables were the logarithm of the relative region volume and the difference between the clinical variable and its baseline value. The only predictor was Δt. It was tested whether the covariance of the random effect estimates of both response variables was significantly different from zero.
- Because several recent studies had examined associations between cognitive and structural changes by comparing groups of cognitively normal, mildly impaired and demented patients, we conducted an additional analysis by subdividing the present sample of PD patients in a group of cognitively stable or declining subjects. Regional differences of volume change rates of both groups were analyzed by a univariate linear mixed model in the same ways as in the comparison of patients and

reference template. (G) Brain atlas transformed into the source image, i.e., the baseline image of each subject. (H–M) Longitudinal processing of MR images to detect local volume changes: Structural changes in the longitudinal series of MR images of each subject are detected by a symmetrical registration of each follow-up image with the baseline image (H) Baseline MR image of a subject. (I) Follow-up MR images of the same subject. The baseline image is registered with each of the follow-up images. (J) Deformation field of the non-linear registration. The vectors are stretched by a factor of 14 to improve their visibility. (K) Enlargement of the marked region in (J) in the affinely matched baseline and follow-up image. The region covers the amygdala. The corresponding deformation vectors are superimposed on each image. The vectors are stretched by a factor of four relative to the image voxel sizes. The time difference between the acquisition time points of both MR images was 8.5 years. Note that the calculated deformations are much smaller than the voxel sizes. (L) Map of relative volume changes (= Local Volume Ratio, LVR) corresponding to the deformation field shown in (J). Volume changes >4% are visualized (shrinkage in red–yellow, expansion in blue). (M) The LVR maps are transformed into the native space of the baseline MR image of each subject. The Julich-Brain atlases and other maps are also transformed onto the baseline images. E.g., maps of nuclei in the amygdala are shown in green. Relative volume changes of *brain regions* are calculated for each subject and time point by averaging of the LVR data over each region.

controls (see Supplemental material, paragraph "Cognitive changes of PD patients").

These analyses were carried out using the software SAS 9.4 (SAS Institute, Cary, NC).

2.5.3. *Control of type I error*

The statistical models were examined separately for 205 brain regions in each hemisphere and 16 midline regions. To control the increased type I error risk, we applied a hierarchical method for the estimation of the false discovery rate (FDR) (Benjamini & Hochberg, 1995). Similar methods had been proposed in recent years especially for studies which examined hundreds or even more hypotheses (Benjamini & Bogomolov, 2014; Yekutieli, 2008): The hypotheses are divided into "families", a p-value is calculated for each family, and the FDR is calculated for these p-values, so that significant family-effects can be selected. Nineteen region families were defined (frontal, parietal, occipital and temporal lobes, cerebellum, cingulate gyrus, insula, basal ganglia, thalamus in each hemisphere, and bilateral brainstem, see Supplemental Table 1 and Supplemental Fig. 1), and all regions of the Julich-Brain and AAL3 atlas were assigned to one of these families. Then the FDR was calculated for the p-values of the hypotheses within each selected family, however, with a reduced FDR threshold:

$$q_{\text{within}} = q\, S_f / N_f$$

(S_f = number of selected families, N_f = number of all families, q = global FDR threshold, e.g., .05). Simes's p-value (Simes, 1986) is often used as a family p-value. In this study, however, the "families" are formed by combined anatomical brain regions, therefore we calculated the volumes of these region-families (or their volume changes), and tested their group differences as before.

3. Results

3.1. *Longitudinal changes of clinical scores*

The UPDRS-III and PDQ-39 in PD patients increased significantly over time (UPDRS-III: 1.6/year, $p < .0002$; PDQ-39: 4.3/year, $p < .0058$). At baseline, all participants were cognitively normal or at most mildly affected (MMSE $\geq$ 24, Table 1). One patient had a strong deterioration in the MMSE from 27 to 14 over a period of 5 years, whereas the MMSE of all other patients and of all controls varied within the range of 3 points over their observation periods. The estimated MMSE change rate in the patients was not significant (−.19/year, $p = .061$). Because the patient with the particularly strong decrease in MMSE had a disproportionately large impact on the longitudinal association analyses of clinical scores and regional volume changes, his data were excluded from all longitudinal association analyses.

3.2. *Group differences of baseline regional volumes*

The volumes of several brain regions were at baseline smaller in PD patients than in controls (Table 2, Fig. 2A). This involved areas in the motor cortex (4P, 6D3), somatosensory area 3A, areas in the intraparietal sulcus, but also areas in the orbitofrontal cortex (FO4, FO5), inferior frontal sulcus (IFJ1/2, IFS1), and frontal and parietal operculum (OP1/5/9), and regions of the hippocampus and entorhinal cortex, among others. Notably, the bilateral pars reticulata of the substantia nigra (SNpr) and left subthalamic nucleus (STN) were also diminished in PD patients. On the other hand, the volumes of some regions were larger in patients than in controls: areas of the insula, right area 7A, and the left cerebellar crus-1 and right thalamic pulvinar. The statistical significance of most effects was moderate (p-values .01−.05), and the multiple testing criterion was not met. The whole brain or ventricle volume did not differ significantly between the two groups at baseline, but the global white matter showed a smaller volume in PD patients than in controls.

3.3. *Group differences of longitudinal regional volume change rates*

PD patients showed a significantly accelerated decline of the whole brain volume ($p = .0289$, Table 3), with estimated rates of −.33%/year (PD) and −.14%/year (controls). The strongest accelerations of volume declines in patients occurred in the temporal lobe, neighboring parts of the inferior parietal lobe and ventral parts of the frontal lobe, while more dorsally located parts of the brain were less involved and did not reach significance (Fig. 3A). Pronounced inter-hemispheric differences were not observed. The volume decline could be attributed to the gray matter compartment ($p = .0002$), whereas the volume changes of the global white matter did not differ significantly between groups ($p = .6864$). The lateral ventricles expanded faster in the PD group than in controls with change rate differences of 1.8% ($p = .028$) and 1.7% ($p = .047$) in the left and right hemisphere. These data are compiled in Table 3 and shown in Figs. 3A and 4. Supplemental Fig. 2 shows the differences of the annual relative volume changes between both groups.

In more detail: Significant differences in volume decline were found in the lateral and ventral occipital lobe, in particular in cytoarchitectonic areas FG1/2/4 of the fusiform gyrus, extrastriate areas hOC2-5 (Caspers et al., 2013; Lorenz et al., 2015; Malikovic et al., 2016; Rottschy et al., 2007), in the temporal lobe with primary and higher auditory areas on the superior temporal gyrus and sulcus (TE10/21/3, STS1/2) (Morosan et al., 2001; Zachlod et al., 2020), the hippocampus and amygdala (Amunts et al., 2005; Palomero-Gallagher, Kedo, Mohlberg, Zilles, & Amunts, 2020). Further differences were found in areas FO3/6/7 of the medial and lateral orbitofrontal cortex (Henssen et al., 2016; Wojtasik et al., 2020), the left inferior frontal cortex including areas 44 and 45 of Broca's region (Amunts et al., 1999), the nucleus basalis Meynert (CH4 group) (Zaborszky et al., 2008), the parietal lobe areas PF, PG (Caspers et al., 2008), 7P, 5CI (Scheperjans et al., 2008), the insula with dysgranular areas ID4-10 and granular area IG2, as well as the putamen, pallidum, locus coeruleus and ventral tegmental area.

The FDR-based multiple-testing criterion was fulfilled by nine region families (i.e., BRAINSTEM, CEREBELLUM-L, FRONTAL-L, INSULA-L/R, OCCIPITAL-L/R, TEMPORAL-L/R)

Table 2 – Differences of baseline volumes between PD patients and controls. Results of those regions are shown where the uncorrected *p*-value of the ANCOVA estimate of the group difference is equal or below .05, and the results of the superordinate region families. % Volume-diff., t-value, *p*-value: Estimated percentual region volume difference (controls – PD patients, in mm^3) and uncorrected statistical scores. FDR: Estimated false-discovery rate. The first row of each region family shows the estimates and scores of the whole region family. Note that the FDR was calculated differently for anatomical regions and superordinate region families. CLS: Atlas of global tissue classes in the Colin27-brain. AAL3: AAL3 atlas. Julich-Brain: Julich-Brain-Atlas. The suffix "_L" and "_R" indicate the hemisphere of each region.

Region family	Atlas	Region	% Volume diff.	t-value	*p*-value (uncorr.)	FDR
	BRAIN	BRAIN	1.22	1.66	.1000	
	BRAIN	BRAIN_L	1.21	1.63	.1064	
	BRAIN	BRAIN_R	1.24	1.68	.0969	
	VENTRICLES	VENTRICLE_3	3.32	.44	.6589	
	VENTRICLES	VENTRICLE_4	−1.86	−.31	.7603	
	VENTRICLES	VENTRICLE_LAT_L	10.16	1.38	.1720	
	VENTRICLES	VENTRICLE_LAT_R	8.49	1.09	.2779	
	CLASSES	CSF	1.85	1.72	.0887	
	CLASSES	GM	.97	1.39	.1681	
	CLASSES	WM	1.89	2.02	.0462	
BASAL_GANGLIA_L	–	BASAL_GANGLIA_L	1.36	1.24	.2195	.4635
	AAL3	SN_pr_L	3.32	2.32	.0227	.1239
BASAL_GANGLIA_R	–	BASAL_GANGLIA_R	1.48	1.34	.1823	.4635
	AAL3	SN_pr_R	2.98	2.03	.0455	.1485
CEREBELLUM_L	–	CEREBELLUM_L	−.07	−.06	.9556	.9917
	AAL3	Cerebellum_Crus1_L	−3.96	−2.17	.0328	.5237
FRONTAL_L	–	FRONTAL_L	.79	.83	.4058	.7010
	Julich-Brain	IFS_IFJ1_L	5.28	2.06	.0424	.3023
	Julich-Brain	IFS_IFJ2_L	6.55	2.25	.0264	.2433
	Julich-Brain	Motor_4P_L	6.13	2.66	.0092	.2106
	Julich-Brain	OFC_FO4_L	5.14	2.31	.0228	.2433
	Julich-Brain	Operculum_OP1_L	5.14	2.36	.0202	.2433
	Julich-Brain	Premotor_6D3_L	6.89	3.03	.0032	.1463
FRONTAL_R	–	FRONTAL_R	1.44	1.50	.1358	.4301
	Julich-Brain	FrontalPole_FP2_R	4.43	2.10	.0383	.2518
	Julich-Brain	GapMap_FRONTAL-I_R	2.65	2.03	.0451	.2595
	Julich-Brain	IFS_IFS1_R	8.15	2.30	.0236	.2435
	Julich-Brain	OFC_FO4_R	5.65	2.18	.0318	.2435
	Julich-Brain	OFC_FO5_R	5.93	2.28	.0249	.2435
	Julich-Brain	Operculum_OP5_R	4.28	2.29	.0241	.2435
	Julich-Brain	Operculum_OP9_R	5.00	2.25	.0268	.2435
	Julich-Brain	SFG_8D2_R	5.56	2.20	.0306	.2435
INSULA_L	–	INSULA_L	−.53	−.50	.6156	.8997
	Julich-Brain	Insula_ID2_L	−8.06	−3.24	.0016	.0263
	Julich-Brain	Insula_ID5_L	−4.20	−2.59	.0110	.0789
	Julich-Brain	Insula_ID7_L	5.07	2.11	.0372	.1191
	Julich-Brain	Insula_ID9_L	−5.92	−2.48	.0148	.0789
	Julich-Brain	Insula_IG2_L	−4.46	−2.12	.0365	.1191
INSULA_R	–	INSULA_R	.47	.42	.6729	.8999
	Julich-Brain	Insula_ID2_R	−7.77	−3.67	.0004	.0063
	Julich-Brain	Insula_ID7_R	6.55	2.68	.0086	.0688
OCCIPITAL_L	–	OCCIPITAL_L	2.00	1.59	.1149	.4301
	Julich-Brain	Visual_FG3_L	3.45	2.23	.0283	.1322
	Julich-Brain	Visual_HOC4LP_L	4.02	2.32	.0224	.1322
	Julich-Brain	Visual_HOC5_L	5.67	2.26	.0263	.1322
PARIETAL_L	–	PARIETAL_L	1.19	1.27	.2066	.4635
	Julich-Brain	AIPS_IP2_L	9.47	2.92	.0043	.0626
	Julich-Brain	PSC_3A_L	4.61	3.07	.0028	.0626
PARIETAL_R	–	PARIETAL_R	.49	.52	.6063	.8997
	Julich-Brain	PIPS_HIP5_R	4.66	2.14	.0351	.2497
	Julich-Brain	PIPS_HIP6_R	5.81	1.99	.0495	.2497
	Julich-Brain	PSC_3A_R	4.84	3.22	.0018	.0510
	Julich-Brain	SPL_7A_R	−4.35	−2.11	.0378	.2497
TEMPORAL_L	–	TEMPORAL_L	1.79	2.08	.0407	.4003
	Julich-Brain	Auditory_STS2_L	5.51	2.74	.0074	.2013
	Julich-Brain	Auditory_TPJ_L	6.39	2.27	.0252	.2013
	Julich-Brain	Hippocampus_CA1_L	3.10	2.18	.0314	.2013
	Julich-Brain	Hippocampus_EC_L	5.13	2.30	.0239	.2013
	Julich-Brain	Hippocampus_PROS_L	5.84	2.23	.0279	.2013

(*continued on next page*)

Table 2 – (*continued*)

Region family	Atlas	Region	% Volume diff.	t-value	*p*-value (uncorr.)	FDR
TEMPORAL_R	–	TEMPORAL_R	1.73	2.02	.0460	.4003
	Julich-Brain	Auditory_STS2_R	4.46	2.25	.0268	.2898
	Julich-Brain	Auditory_TE11_R	5.19	2.04	.0445	.2898
	Julich-Brain	GapMap_TEMPORAL-TO-PARIETAL_R	2.23	2.09	.0389	.2898
	Julich-Brain	Hippocampus_EC_R	6.91	3.03	.0031	.1004
THALAMUS_L	–	THALAMUS_L	−.01	−.01	.9917	.9917
	Julich-Brain	Thalamus_CGL_L	2.94	2.35	.0207	.2268
	Julich-Brain	Thalamus_STN_L	3.33	2.27	.0252	.2268
THALAMUS_R	–	THALAMUS_R	−.46	−.35	.7241	.8999
	AAL3	Thal_PuM_R	−3.64	−2.02	.0467	.3299

and several areas within these families (FDR threshold: $0.05 \cdot 9/19 = 0.0237$).

In addition to these group-level analyses, Fig. 4 shows individual trajectories of different brain region volumes as line plots to visualize differences between PD patients and controls: The average decline of patients was steeper than in controls in several brain regions. Moreover, the intersubject variability in the group of patients appeared to be larger than in the group of controls. Please note that the time axis indicates the interval since the baseline examination of each subject, but not the disease duration (baseline disease duration 3.7 ± 2.3 years).

The spatio-temporal pattern of progressive volume loss in PD is exemplarily shown for a patient brain, where voxel-wise volume changes are visualized (baseline age 44.0 years, disease duration 2.4 years): The patient was scanned eleven times over a period of 8.5 years (Fig. 5A). Over time, growing parts of the brain show a local volume loss of more than 4% relative to the baseline, as indicated by red voxels. Contiguous clusters of volume loss above this threshold can be found already after 2.6 years in the amygdala and medial temporal lobe, but also in the frontal lobe. These clusters grow mainly in the basal ganglia, temporal lobe and lateral frontal lobe. Brain tissue shrinkage affects mainly the gray matter with the cerebral cortex and subcortical nuclei, while the white matter seems to be less affected.

3.4. *Associations of brain region volumes and clinical scores*

All significant correlations of clinical scores with the patients' baseline volume data are listed in Table 4, and the longitudinal covariances between clinical score and regional volume change rates in Table 5. They are visualized in Fig. 2B–D and Fig. 6.

Negative correlations of the patients' baseline residual volume data with the UPDRS-III were found in the left orbitofrontal area FO6, left inferior parietal areas PF, PFCM, PFOP, area HIP4 of the intraparietal sulcus, and left lateral occipital cortex (HOC4, HOC5). Additional correlations were found in the dentate nucleus and the vermis of the cerebellum. Positive associations were found in area HIP8 of the intraparietal sulcus and in area TPJ at the junction of the parietal and temporal lobe. The longitudinal analyses indicated a negative covariance of region volume and UPDRS-III changes in the amygdala, hippocampus, entorhinal cortex, cerebellum and thalamus (mediodorsal nucleus (MD), lateral geniculate nucleus (LGN)) (Table 5). A negative covariance of longitudinal volume decline and UPDRS-III means that a faster UPDRS-III increase is associated with an accelerated volume decline, given that most regions undergo a longitudinal volume decline.

Both, the baseline and longitudinal association analyses of the PDQ-39 with the region volumes (and their changes) yielded almost exclusively negative associations, indicating that an increase of the PDQ-39 is associated with decline of region volumes. At baseline, significant associations were found in the orbitofrontal (FO3), inferior frontal (left areas 44 and 45 of Broca's region), and frontal opercular (OP6/8/9) cortex, but also in the dorsal premotor cortex (6D2, 6D3) and frontal pole, as well as in areas mainly in the left parietal and occipital lobes. Negative longitudinal associations of the PDQ-39 were found in the dorsal premotor cortex, in the cingulate cortex (area 25, 33) (Palomero-Gallagher et al., 2015), medial temporal lobe (amygdala, hippocampus) and right nucleus accumbens and nucleus basalis Meynert. Only the following cerebellar regions showed a positive longitudinal association with the PDQ-39 changes: Lobule VIII, dentate and fastigial nuclei.

A few areas in the parietal lobe (right 7P, left PGa), temporal lobe (left parahippocampal area PH3) and in the cerebellum showed positive associations with the MMSE in the baseline analysis, while other areas in frontal, parietal and cingulate lobes were negatively associated (IFJ1, OP2, SMA, 5M, S32; see Table 4). The longitudinal association analysis indicated positive covariances of MMSE changes with regions in the right temporal lobe (e.g., amygdala, entorhinal cortex, subiculum, transsubiculum), frontal operculum (OP8), orbitofrontal cortex (FO5/6), premotor area 6D2, nucleus accumbens, and with cingulate area 25. In addition, the thalamic nuclei MD, LGN, VPL and VA had a positive association. The group comparison of regional volume change rates between cognitively stable and declining PD patients suggests, that the later had stronger atrophy mainly in the dorsal and lateral cortex (e.g., superior parietal lobule, primary motor cortex, premotor cortex) but also in the amygdala, insular cortex and left hippocampus. On the other hand, cognitively stable PD patients had stronger atrophy in the basal ganglia, thalamus, anterior cingulate gyrus, but also in the ventral occipital lobe and brainstem (see Supplemental Fig. 4).

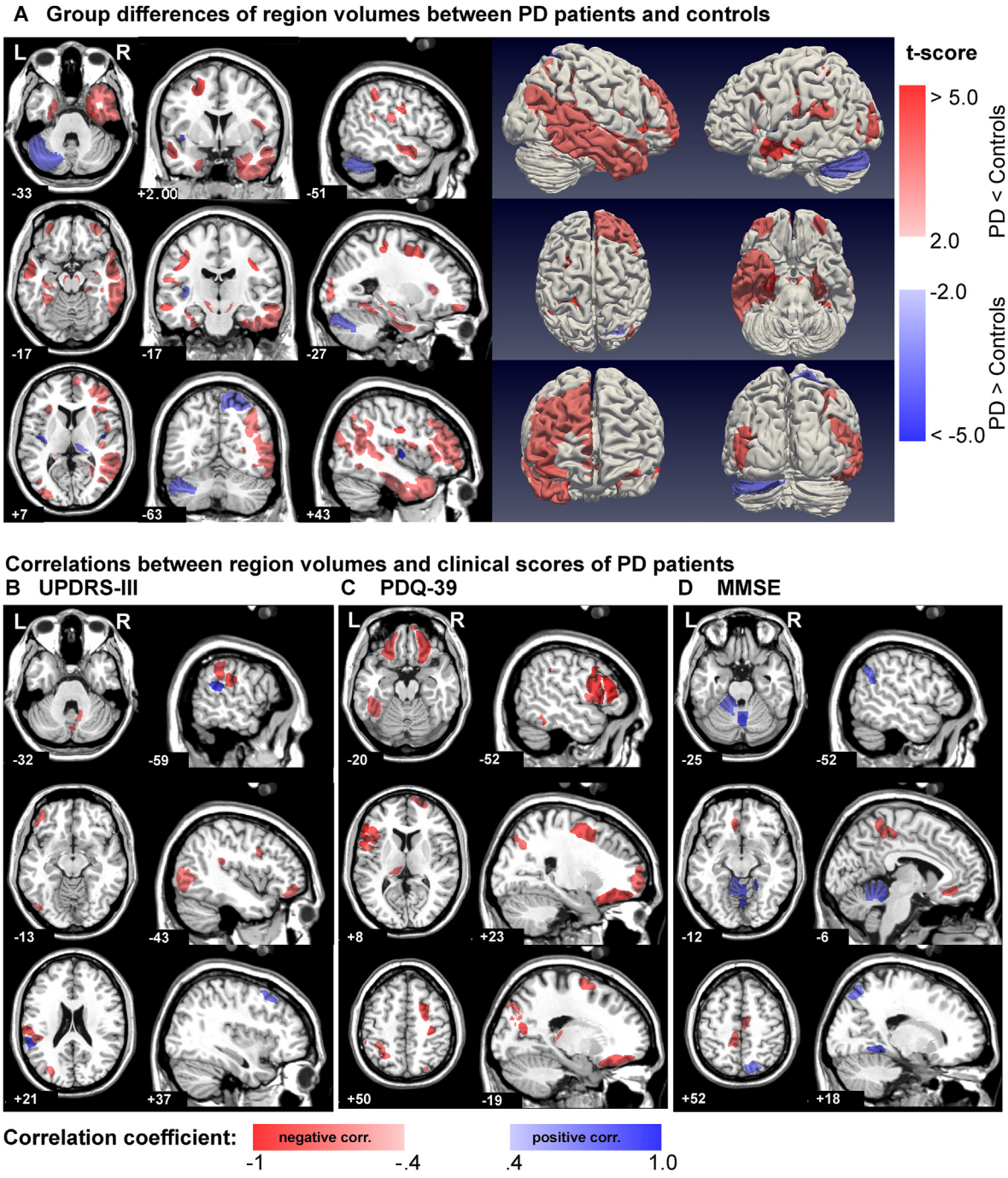

Fig. 2 – Results of the baseline analysis of the brain region volumes. Those regions in the reference brain (Colin27) are colored where significant statistical effects had been found. (A) Group differences between PD patients and controls in region volumes at baseline. Volume loss of PD patients are in red, and enlargements in blue. The transparency indicates the effect strength. The first three columns show horizontal, coronal and sagittal sections, and columns four and five surface reconstructions. (B) Correlations of region volumes of PD patients with UPDRS-III score (motor examinations). Regions with significant negative correlations are colored in red, and positive correlations in blue. (C) Correlations with PDQ-39. (D) Correlations with MMSE. Note that decreasing MMSE scores indicate a worse condition.

4. Discussion

The present study examined MR images obtained from PD patients and controls over several years using Deformation-Based-Morphometry and analyzed regional changes of brain structure based on neuroanatomical atlases. It showed accelerated longitudinal volume decreases in PD patients in comparison with controls, in particular in the gray matter. The evaluation of neuroanatomically defined brain regions revealed a specific spatio-temporal pattern of changes in

Table 3 – Longitudinal regional differences between PD patients and controls. Results of those regions are shown where the false discovery rate (FDR) was equal or below .05, and results of superordinate region families and global maps. Volume change diff.: Difference between groups (controls – PD patients) in regional volume change rates, measured in percent/year. t-value, *p*-value: Uncorrected scores of statistical tests. FDR: Estimated false-discovery-rate. NBM: nucleus basalis Meynert.

Region family	Atlas	Region	Volume change diff.	t-value	*p*-value (uncorr.)	FDR
	BRAIN	BRAIN	.1904	2.1938	.0289	
	BRAIN	BRAIN_L	.2078	2.1802	.0299	
	BRAIN	BRAIN_R	.1684	2.0933	.0370	
	CLASSES	CSF	−.2768	−2.3385	.0199	
	CLASSES	GM	.2485	3.7729	.0002	
	CLASSES	WM	.0394	.4041	.6864	
	VENTRICLES	VENTRICLE_3	−.1334	−.2548	.7990	
	VENTRICLES	VENTRICLE_4	.2742	.5537	.5801	
	VENTRICLES	VENTRICLE_LAT_L	−1.8011	−2.2062	.0280	
	VENTRICLES	VENTRICLE_LAT_R	−1.6689	−1.9942	.0469	
BASAL_GANGLIA_L	–	BASAL_GANGLIA_L	.3454	1.7644	.0785	.1113
	AAL3	Putamen_L	.5118	2.0776	.0385	.2309
BASAL_GANGLIA_R	–	BASAL_GANGLIA_R	.2033	1.1569	.2481	.2619
	AAL3	Pallidum_R	.5158	2.1689	.0308	.1846
BRAINSTEM	–	BRAINSTEM	.2453	2.5114	.0125	.0306
	AAL3	LC_L	.4724	2.5161	.0123	.0739
	AAL3	VTA_L	.5341	2.1597	.0315	.0944
CEREBELLUM_L	–	CEREBELLUM_L	.2223	2.5980	.0098	.0306
	AAL3	Cerebellum_8_L	.4874	2.0656	.0396	.3565
	AAL3	Cerebellum_9_L	.4066	2.2957	.0223	.3565
FRONTAL_L	–	FRONTAL_L	.1963	2.4828	.0135	.0306
	Julich-Brain	Bforebrain_4_L	.6061	2.5690	.0106	.1115
	Julich-Brain	Broca_44_L	.3774	3.1059	.0021	.0945
	Julich-Brain	Broca_45_L	.3755	2.3921	.0173	.1115
	Julich-Brain	GapMap_FRONTAL-II_L	.2241	2.4809	.0136	.1115
	Julich-Brain	GapMap_FRONTAL-TO-OCCIPITAL_L	.2271	2.3490	.0194	.1115
	Julich-Brain	GapMap_FRONTAL-TO-TEMPORAL-I_L	.3537	2.5312	.0118	.1115
	Julich-Brain	OFC_FO3_L	.3278	2.2952	.0223	.1141
	Julich-Brain	OFC_FO6_L	.3391	2.1931	.0290	.1332
	Julich-Brain	OFC_FO7_L	.2783	2.4317	.0155	.1115
	Julich-Brain	Operculum_OP1_L	.2165	2.0244	.0437	.1772
	Julich-Brain	Operculum_OP4_L	.2328	2.4705	.0140	.1115
	Julich-Brain	Operculum_OP6_L	.1894	2.0005	.0462	.1772
FRONTAL_R	–	FRONTAL_R	.1686	2.0198	.0442	.0763
	Julich-Brain	Bforebrain_4_R	.4985	3.5476	.0004	.0203
	Julich-Brain	GapMap_FRONTAL-TO-OCCIPITAL_R	.2082	2.4737	.0138	.1593
	Julich-Brain	OFC_FO3_R	.4858	2.5593	.0109	.1593
	Julich-Brain	OFC_FO7_R	.6776	3.0394	.0026	.0587
	Julich-Brain	Operculum_OP4_R	.3073	2.1501	.0322	.2966
INSULA_L	–	INSULA_L	.3498	3.1515	.0018	.0087
	Julich-Brain	Insula_ID10_L	.3257	2.6047	.0096	.0506
	Julich-Brain	Insula_ID4_L	.4251	2.3672	.0185	.0506
	Julich-Brain	Insula_ID6_L	.3342	2.4538	.0146	.0506
	Julich-Brain	Insula_ID7_L	.4113	2.3529	.0192	.0506
	Julich-Brain	Insula_ID8_L	.5133	2.6148	.0093	.0506
	Julich-Brain	Insula_ID9_L	.3525	2.2984	.0221	.0506
	Julich-Brain	Insula_IG2_L	.4646	2.3031	.0219	.0506
INSULA_R	–	INSULA_R	.3014	2.6159	.0093	.0306
	Julich-Brain	Insula_ID5_R	.4663	2.0737	.0388	.1430
	Julich-Brain	Insula_ID6_R	.2688	1.9954	.0468	.1430
	Julich-Brain	Insula_ID8_R	.2942	2.6940	.0074	.0592
	Julich-Brain	Insula_IG2_R	.3354	3.2149	.0014	.0228
OCCIPITAL_L	–	OCCIPITAL_L	.1786	2.4577	.0145	.0306
	Julich-Brain	Visual_FG2_L	.4184	2.7471	.0063	.0342
	Julich-Brain	Visual_FG4_L	.3724	2.6978	.0073	.0342
	Julich-Brain	Visual_HOC2_L	.2072	2.1149	.0352	.0984
	Julich-Brain	Visual_HOC4LA_L	.5517	3.6368	.0003	.0045
	Julich-Brain	Visual_HOC4LP_L	.4057	2.1843	.0296	.0984

Table 3 – (*continued*)

Region family	Atlas	Region	Volume change diff.	t-value	*p*-value (uncorr.)	FDR
OCCIPITAL_R	–	OCCIPITAL_R	.1966	3.1400	.0018	.0087
	Julich-Brain	Visual_FG1_R	.3022	3.2001	.0015	.0210
	Julich-Brain	Visual_FG2_R	.2819	2.1609	.0314	.0549
	Julich-Brain	Visual_FG4_R	.2256	2.3712	.0183	.0495
	Julich-Brain	Visual_HOC2_R	.2033	2.5417	.0115	.0401
	Julich-Brain	Visual_HOC3V_R	.2630	2.7628	.0060	.0362
	Julich-Brain	Visual_HOC4LA_R	.2494	2.6780	.0078	.0362
	Julich-Brain	Visual_HOC4LP_R	.2341	2.2551	.0247	.0495
	Julich-Brain	Visual_HOC4V_R	.2357	2.2720	.0237	.0495
	Julich-Brain	Visual_HOC5_R	.3472	2.0824	.0380	.0592
PARIETAL_L	–	PARIETAL_L	.1583	2.0852	.0378	.0718
	Julich-Brain	IPL_PFM_L	.4479	3.5175	.0005	.0134
	Julich-Brain	IPL_PF_L	.3118	2.6840	.0076	.0553
	Julich-Brain	IPL_PGA_L	.3818	3.3417	.0009	.0134
	Julich-Brain	IPL_PGP_L	.3809	3.0977	.0021	.0204
	Julich-Brain	SPL_7P_L	.4017	2.3942	.0172	.0997
PARIETAL_R	–	PARIETAL_R	.1344	1.5249	.1282	.1522
	Julich-Brain	IPL_PGP_R	.2583	2.1218	.0346	.3508
	Julich-Brain	PSC_2_R	.2255	1.9810	.0484	.3508
	Julich-Brain	SPL_5CI_R	.1982	2.0423	.0419	.3508
	Julich-Brain	SPL_7P_R	.3924	2.1965	.0287	.3508
TEMPORAL_L	–	TEMPORAL_L	.3579	3.8369	.0001	.0014
	Julich-Brain	Amygdala_SF_L	.5828	2.6595	.0082	.0386
	Julich-Brain	Auditory_STS1_L	.2413	2.0532	.0408	.1485
	Julich-Brain	Auditory_STS2_L	.4870	2.9658	.0032	.0178
	Julich-Brain	Auditory_TE10_L	.3931	2.2910	.0226	.0931
	Julich-Brain	Auditory_TE21_L	.2057	2.0118	.0450	.1485
	Julich-Brain	Auditory_TE3_L	.5022	3.8429	.0001	.0037
TEMPORAL_L	Julich-Brain	Auditory_TPJ_L	.4142	3.5469	.0004	.0049
	Julich-Brain	CollateralSulcus_COS1_L	.4651	3.3046	.0011	.0087
	Julich-Brain	GapMap_TEMPORAL-TO-PARIETAL_L	.4124	3.7271	.0002	.0037
	Julich-Brain	Parahippocampal_PH2_L	.3597	3.0359	.0026	.0170
TEMPORAL_R	–	TEMPORAL_R	.3139	3.9445	.0001	.0014
	Julich-Brain	Amygdala_LB_R	.4074	2.6167	.0093	.0510
	Julich-Brain	Amygdala_SF_R	.8523	2.7508	.0063	.0510
	Julich-Brain	Auditory_STS1_R	.2388	2.3132	.0213	.0858
	Julich-Brain	Auditory_STS2_R	.2926	2.8756	.0043	.0471
	Julich-Brain	Auditory_TE10_R	.2254	2.0974	.0367	.1211
	Julich-Brain	Auditory_TE11_R	.7251	2.6565	.0083	.0510
	Julich-Brain	Auditory_TE22_R	.2163	2.2769	.0234	.0858
	Julich-Brain	CollateralSulcus_COS1_R	.3634	1.9994	.0463	.1275
	Julich-Brain	GapMap_TEMPORAL-TO-PARIETAL_R	.3312	3.6230	.0003	.0110
	Julich-Brain	Hippocampus_CA3_R	.3358	2.0011	.0462	.1275
	Julich-Brain	Hippocampus_DG_R	.2946	2.4678	.0141	.0664
	Julich-Brain	Hippocampus_EC_R	.4643	2.8826	.0042	.0471
THALAMUS_L	–	THALAMUS_L	.1809	.9642	.3356	.3356
	AAL3	Thal_MDm_L	.5208	2.1115	.0354	.5309
THALAMUS_R	–	THALAMUS_R	.2880	1.7443	.0820	.1113
	AAL3	Thal_PuI_R	.6547	2.1883	.0293	.3243

brains of PD patients, which was different from healthy aging. The most pronounced group differences in volume change rates were found in the ventral parts of occipital, temporal and orbitofrontal cortices, in addition in the insular and parietal cortices, whereas the dorsal frontal cortex was relatively spared.

The baseline analysis of volume differences between both groups provides information about atrophy, which occurred already before the first examination of the subjects. The pattern of occipital, temporal and inferior frontal regions with reduced volumes in PD patients at baseline fits in the pattern of regions which show volume change differences in the longitudinal analysis (Figs. 2A, 3A). However, the baseline analysis revealed also significant volume differences of some regions where no longitudinal differences were found: Among these were in particular the SNpr, STN, areas 4P and 6D3 of the motor cortex, which belong to motor circuits putatively affected in PD (Peterson & Horak, 2016), and dorsal area 8D2. A histological study which counted neurons in the pars compacta of the SN suggested that the neuron number declines exponentially in PD, and that at symptom onset already about 31% of neurons could be degenerated due to PD, i.e., in addition to age-related losses (Fearnley & Lees, 1991). Assuming a similar decline for the SNpr, this could explain the lack of a longitudinal effect in this region. The volume enlargements of the cerebellar crus-1, right parietal area 7A, and insular areas

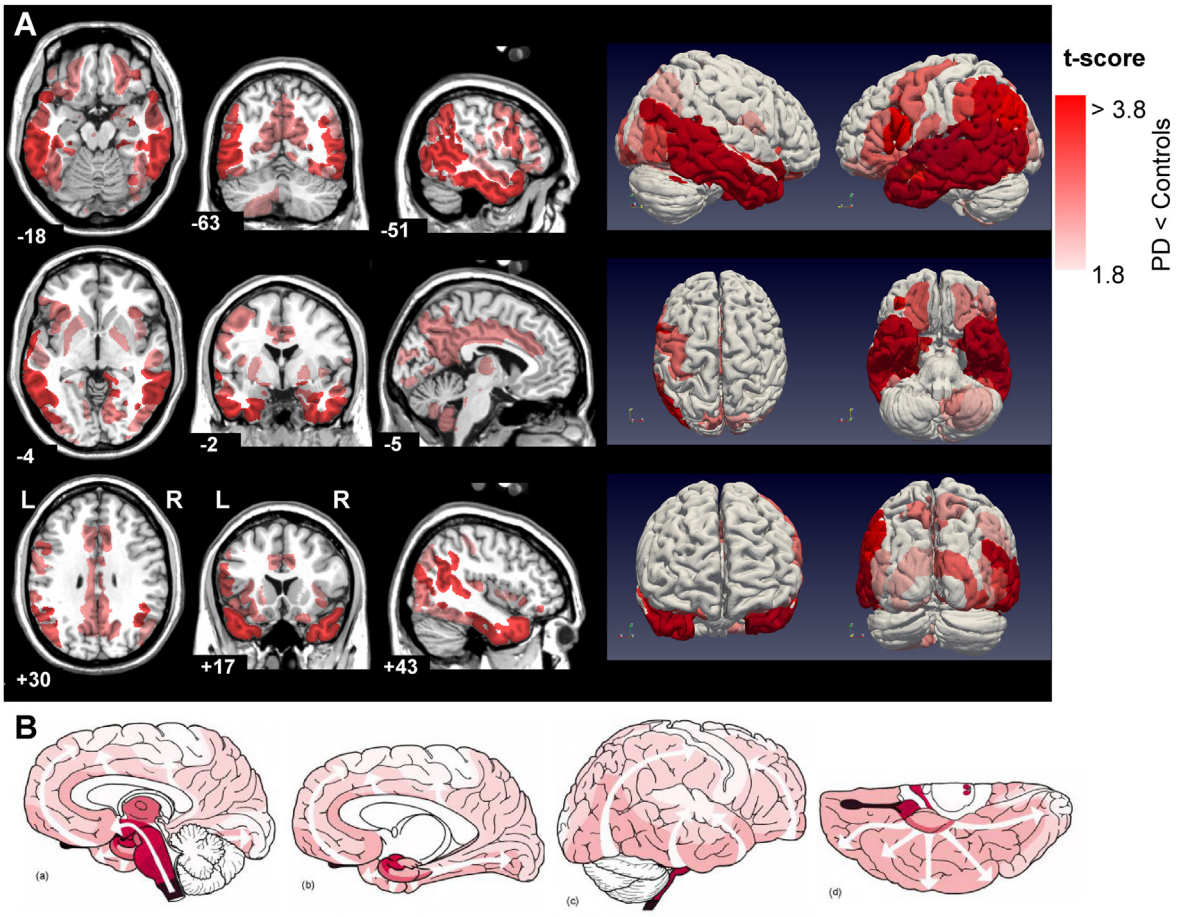

Fig. 3 – Results of the longitudinal analysis of brain region volumes. Those regions in the reference brain (Colin27) are colored where significant statistical effects had been found. Regions in the brain of both, patients and controls, decline over time, however, volume declines of patients are accelerated in several regions. (A) Group differences between PD patients and controls in rates of longitudinal region volume changes. Regions, where the volume decline of PD patients is accelerated relative to controls, are colored in red. The transparency indicates the effect strength. The first three columns show horizontal, coronal and sagittal sections, and columns four and five surface reconstructions. (B) Scheme of α-synucleinopathy proliferation as suggested by Braak et al. (Reproduction of figure 4 in Braak et al. (2003), with permission), based on the neuropathological examination of post-mortem brains. The color shades indicate the stage, from which on the regions are affected, i.e., the brighter the color of a region, the later it is affected.

in PD patients at baseline are in line with findings of functional MRI studies which suggested compensatory increased activations in particular in the cerebellar and parietal cortex of PD patients in comparison with controls when performing automated movements (Wu & Hallett, 2005, 2013). These compensatory activations are assumed to occur only in the early phase of PD.

The longitudinal in-vivo pattern of accelerated atrophy in brains of PD patients was highly similar to the propagation of αSyn-pathology in PD, as proposed by Braak and colleagues (Braak et al., 2003). The regional pattern of statistical effect strengths as shown in Fig. 3A resembles the staging scheme of αSyn-pathology propagation shown in Fig. 3B (reproduction of Fig. 4 in Braak et al. (2003), with permission). The most pronounced PD-related accelerations of volume shrinkage were found in those brain regions, which were affected by the αSyn-pathology from PD stages 4 and 5 on, whereas the effects in brain regions, which are affected in PD stage 6, were weaker or absent. Because motor symptoms are assumed to occur firstly in PD stages 3 and 4 (Hawkes, Del Tredici, & Braak, 2010), and the average disease duration of our patients at their baseline examination was 3.7 years, it appears that the atrophy observed in the present study occurs in parallel with the spreading of αSyn-pathology in stages 3–5. It should also be noted that despite the long observation periods, the individual courses of atrophy progression did not indicate pronounced deviations from linearity (e.g., steeps or plateaus; Fig. 4), suggesting that the annual atrophy rate was nearly constant over the observation periods.

The volume deficits of patients relative to controls at baseline fit into this staging scheme for the most part. The observed volume deficits in the dorsal frontal and parietal cortices, however, should occur only in the latest stages of this scheme. Similar differences between PD patients and controls had also been found in other imaging studies (Filippi et al., 2020; Mak et al., 2015; Pereira et al., 2014) (see below) in

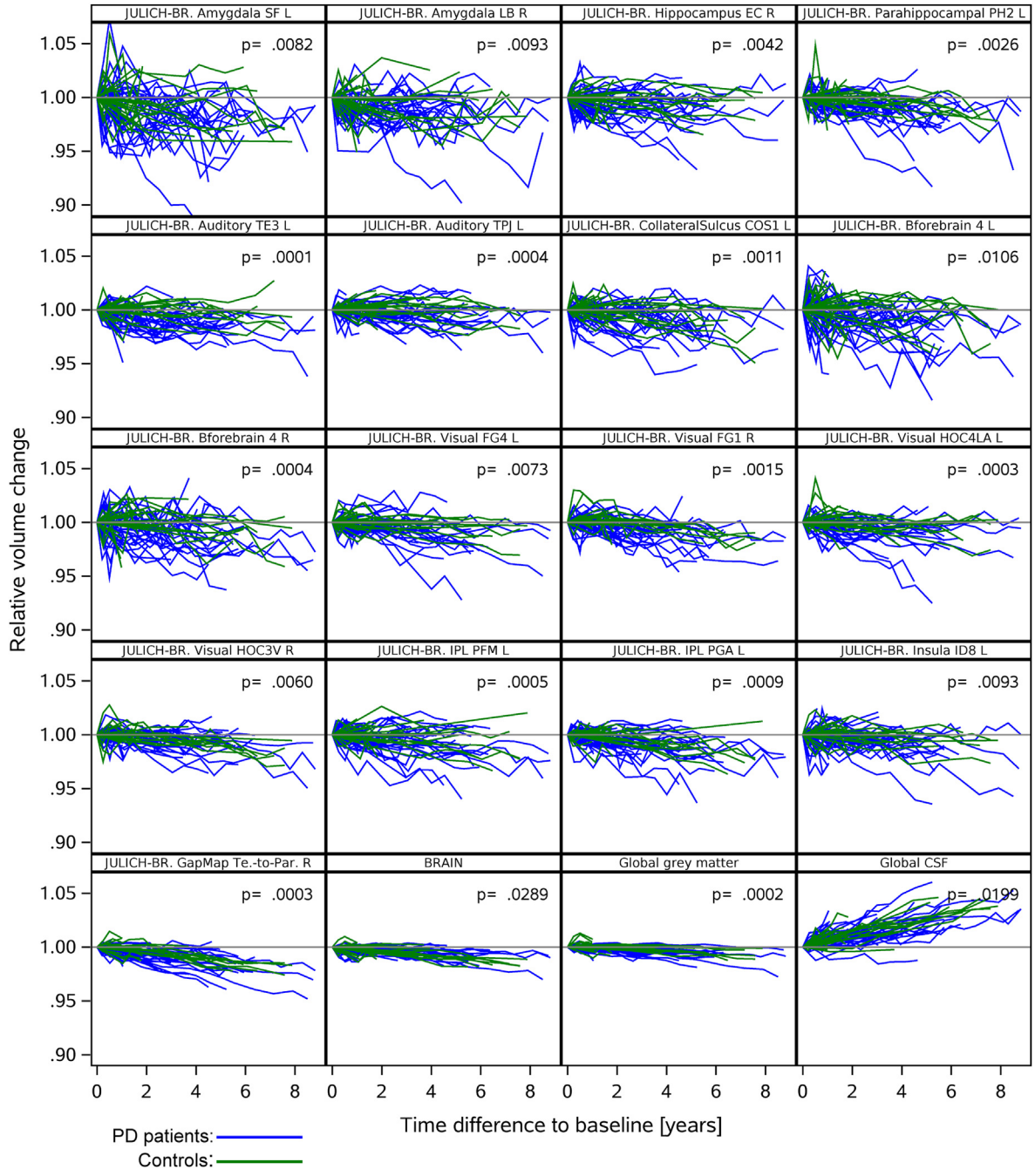

Fig. 4 – Trajectories of individual volume changes of PD patients and controls relative to the baseline MR image (i.e., at t = 0 all relative volumes are equal to one). Blue: PD patients, green: controls. The majority of trajectories have a decreasing tendency. Most severe volume losses are found among patients, and patients show a larger variability than controls. The *p*-value in each plot refers to the group comparison, which was analyzed by a linear mixed model (see also Table 3).

particular in PD patients with cognitive impairments. This observation could indicate that the propagation of αSyn-aggregates starting from the brainstem is not the only pathologic process in PD.

The results at group level can also be observed, to a variable extent, in individual subjects: The pattern of progressive volume changes of an individual subject resembles the propagation of αSyn-pathology in histological sections (Fig. 5; 5B reproduced with permission from Braak et al. (2006)): Both show that the medial temporal lobe and, in particular, the amygdala are affected early, followed by the inferior, lateral and superior temporal cortex, and the insular cortex. Afterwards, parietal, frontal, and cingulate cortices become affected. Such correspondence provides evidence that longitudinal DBM enables to capture structural changes in single individuals during disease progression, whereas in

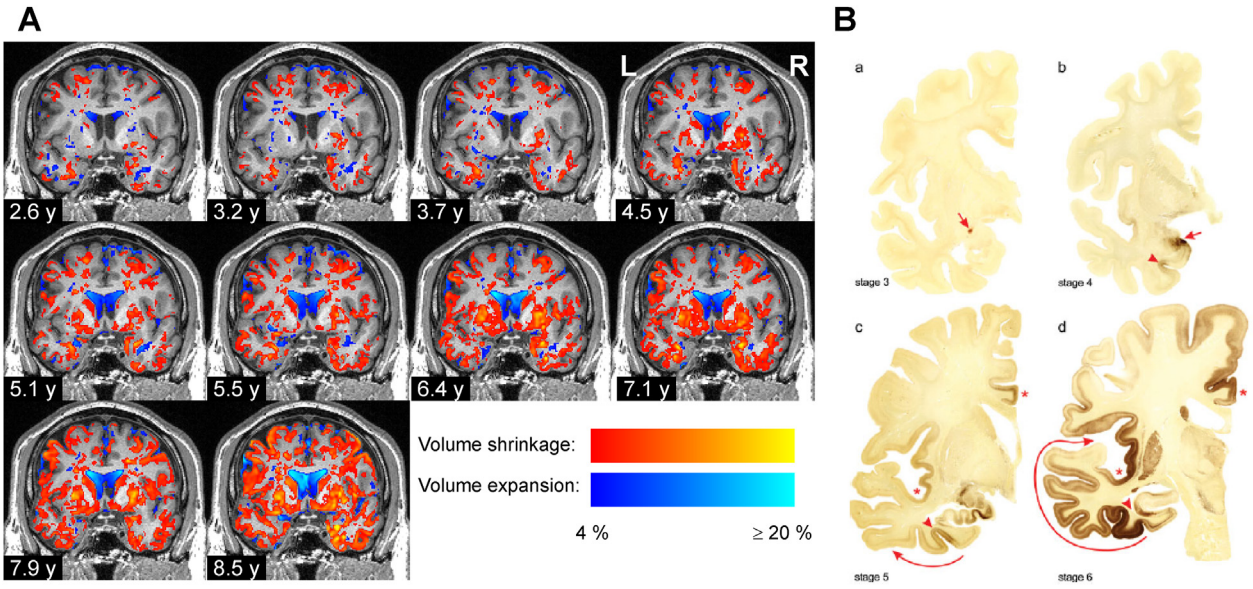

Fig. 5 – Progressive volume atrophy in Parkinson's disease. (A) Longitudinal volume changes in the brain of a PD patient (male, 44 years at baseline) over an observation period of 8.5 years. All images are from the same coronal sections, but at different time points (numbers in lower left corner = difference in years to the baseline MR scan). Volume shrinkage of more than 4% relative to the first time point is indicated by red and yellow; volume increase in blue and cyan (mainly in ventricles and sulci). (B) Histological sections of four post-mortem brains immune-stained for α-synuclein, indicating the spreading of pathological changes in PD (Reproduction of figure 3 in Braak et al. (2006), with permission). Each brain is an example of one PD stage (stage number below each image). The staging scheme was postulated based on comparisons between such post-mortem brains.

neuropathological studies such information can only be indirectly, i.e., cross-sectionally, estimated by comparisons of different post-mortem brains. For clinical applications it could be relevant that the observed pattern of atrophy spread in PD is distinct from that of other neurodegenerative disorders: For example, a previous study of our group in patients with Cortico-Basal Syndrome (CBS) showed that both, the cortex and the deep white matter were affected (Südmeyer et al., 2012). In addition, the cerebellum and pons were less affected in PD than in other, atypical parkinsonian disorders such as Multiple System Atrophy (Wenning, Colosimo, Geser, & Poewe, 2004; Wenning, Tison, Elliott, Quinn, & Daniel, 1996).

Associations of cognitive and motor symptoms with the extent of the αSyn pathology had also been reported in neuropathological studies: A strong association of the neuropathological PD stage with both cognitive and motor symptoms (assessed by MMSE and Hoehn–Yahr score up to 18 months before the subjects' death) was reported in Braak, Rüb, Jansen Steur, Del Tredici, & de Vos (2005). Another neuropathological study (Parkkinen et al., 2008), however, found that in most of their cases the distribution pattern of αSyn – if present – indeed agreed with the PD stages, but 55% of their affected subjects had not presented extrapyramidal motor symptoms or signs of dementia at clinical examinations less than one year before their death. The present study suggests that in patients with manifest PD symptoms progressive atrophy resembling the αSyn spreading (Braak et al., 2006) occurs, which differs from volume changes in healthy controls, but which is not necessarily linked with severe cognitive decline.

Particularly strong accelerations of regional volume decline in PD had been found in areas of the superior and lateral temporal cortex (e.g., TE1/2/3 (Morosan et al., 2001)) and in the ventral occipital cortex (HOC2-4, FG1/2/4 (Amunts, Malikovic, Mohlberg, Schormann, & Zilles, 2000; Kujovic et al., 2013; Malikovic et al., 2016)), in agreement with the αSyn staging scheme. The affected regions are assumed to be involved in auditory and visual processing. Impairments of both functions in PD patients had been demonstrated in several studies (De Groote et al., 2020; Jafari, Kolb, & Mohajerani, 2020; Park & Stacy, 2009; Weil et al., 2016). Visual disturbances involved in particular the functional areas V2–V5, which correspond to the cytoarchitectonic areas HOC2-5 (Amunts et al., 2000; Malikovic et al., 2007). Visual hallucinations also occur in PD, often in conjunction with dementia (Kurita et al., 2019). However, these dysfunctions were not part of the present study, and the examination of their relationship with atrophy remains to be investigated in the future.

The majority of significant associations between clinical scores and baseline region volumes and between their longitudinal changes, which were found in the present study, suggests that worse clinical scores were associated with reduced region volumes. Regarding causal relationships these associations must be interpreted with caution. Moreover, the observed statistical strengths are rather moderate, so that multiple testing corrections were not possible. At the same time all associations were calculated only with the patients' data, so that they were not influenced by the group differences with controls.

Table 4 – Correlations between the residual baseline volumes (from the previous ANCOVA) and clinical scores MMSE, PDQ-39 and UPDRS-III. Results of those regions are shown where the uncorrected *p*-value is equal or below .05. Corr: Pearson-correlation. *p*-value: uncorrected *p*-value of correlation. AAL3: AAL3 atlas. Julich-Brain: Julich-Brain-Atlas. The suffix "_L" and "_R" indicate the hemisphere of each region.

Clinical var.	Region family	Atlas	Region	Corr.	*p*-value
MMSE	CEREBELLUM_L	AAL3	Cerebellum_3_L	.38775	.0214
		AAL3	Cerebellum_4_5_L	.34461	.0426
		AAL3	Vermis_4_5	.40434	.0160
		AAL3	Vermis_6	.48759	.0030
	CINGULATE_GYRUS_L	Julich-Brain	Cingulum_S32_L	−.39352	.0193
	FRONTAL_R	Julich-Brain	IFS_IFJ1_R	−.34201	.0443
		Julich-Brain	Operculum_OP2_R	−.34994	.0393
		Julich-Brain	Supplementarymotor_SMA_R	−.35203	.0381
	PARIETAL_L	Julich-Brain	IPL_PGA_L	.37834	.0250
		Julich-Brain	SPL_5M_L	−.40112	.0169
	PARIETAL_R	Julich-Brain	SPL_7P_R	.34927	.0397
	TEMPORAL_R	Julich-Brain	Parahippocampal_PH3_R	.42344	.0113
PDQ-39		CLASSES	WM	−.37849	.0470
	FRONTAL_L	Julich-Brain	Broca_44_L	−.52375	.0042
		Julich-Brain	Broca_45_L	−.58778	.0010
		Julich-Brain	OFC_FO3_L	−.44742	.0170
		Julich-Brain	Operculum_OP6_L	−.38504	.0430
		Julich-Brain	Operculum_OP8_L	−.37884	.0468
		Julich-Brain	Operculum_OP9_L	−.45578	.0148
		Julich-Brain	Premotor_6D2_L	−.41176	.0295
	FRONTAL_R	Julich-Brain	FrontalPole_FP1_R	−.37799	.0473
		Julich-Brain	Motor_4P_R	−.47495	.0107
		Julich-Brain	OFC_FO3_R	−.48412	.0090
		Julich-Brain	Premotor_6D3_R	−.46331	.0130
	OCCIPITAL_L	Julich-Brain	Visual_FG1_L	−.37913	.0466
		Julich-Brain	Visual_FG4_L	−.39144	.0394
		Julich-Brain	Visual_HOC6_L	−.46195	.0133
	PARIETAL_L	Julich-Brain	AIPS_IP3_L	−.39327	.0384
		Julich-Brain	IPL_PF_L	−.44300	.0182
		Julich-Brain	PIPS_HIP7_L	−.40649	.0318
		Julich-Brain	PIPS_HPO1_L	−.37517	.0492
	PARIETAL_L	Julich-Brain	SPL_7M_L	−.51168	.0054
	PARIETAL_R	Julich-Brain	PIPS_HIP8_R	−.37672	.0482
	THALAMUS_L	AAL3	Thal_PuM_L	−.38130	.0453
UPDRS-3	CEREBELLUM_R	AAL3	Vermis_7	−.42869	.0102
		Julich-Brain	Cerebellum_NDENTV_R	−.34192	.0444
	FRONTAL_L	Julich-Brain	IFS_IFJ2_L	−.34239	.0441
		Julich-Brain	OFC_FO6_L	−.36584	.0307
	FRONTAL_R	Julich-Brain	MFG_8V1_R	.36581	.0307
	OCCIPITAL_L	Julich-Brain	Visual_HOC4LA_L	−.34463	.0426
		Julich-Brain	Visual_HOC5_L	−.34075	.0452
	PARIETAL_L	Julich-Brain	IPL_PFCM_L	−.37281	.0274
		Julich-Brain	IPL_PFOP_L	−.47789	.0037
		Julich-Brain	IPL_PF_L	−.43493	.0090
		Julich-Brain	PIPS_HIP4_L	−.35877	.0343
		Julich-Brain	PIPS_HIP8_L	.34638	.0415
	TEMPORAL_L	Julich-Brain	Auditory_TPJ_L	.50163	.0021
	THALAMUS_R	Julich-Brain	Thalamus_CGM_R	.35266	.0377

The UPDRS-III at baseline had negative associations mainly with regions in the left inferior parietal, occipital and inferior frontal cortex, and it was longitudinally associated with regions in the medial temporal lobe, cerebellum and thalamus. Surprisingly, the UPDRS-III showed the fewest associations with regional volumes among the examined scores. In particular, no associations with the basal ganglia were found, although the longitudinal group comparison indicated an accelerated atrophy of the putamen and pallidum in PD. A reason could be that the patients' medical therapies modulated their motor symptoms without having an impact on the neurodegeneration and on volume changes, particularly as patients were examined in ON-state.

The longitudinal MMSE changes were positively associated with regions in the right medial temporal lobe (superficial nucleus of amygdala, entorhinal cortex, parasubiculum, transsubiculum, dentate gyrus) (Amunts et al., 2005; Palomero-Gallagher et al., 2020), and with the right nucleus accumbens and left cingulate area 25, which are relevant for memory (Aggleton, 2012; Ding, 2013; Lech & Suchan, 2013).

Table 5 – Longitudinal covariance between changes of a clinical variable (MMSE, PDQ-39, UPDRS-III) and the volume change rates of a brain region. Those regions are shown were the covariance parameter was signficantly different from zero (at $p_{uncorr} \leq 0.05$). Corr: Estimated correlation parameter between the clinical variable and the region volume changes. z-value, *p* value: Corresponding statistical scores (uncorrected for multiple testing).

Clinic. var.	Region family	Atlas	Region	Corr.	z-value	*p*-value (uncorr.)
MMSE	CINGULATE_GYRUS_L	Julich-Brain	Cingulum_25_L	.4950	1.97	.0488
	FRONTAL_L	Julich-Brain	OFC_FO5_L	.4852	1.98	.0476
		Julich-Brain	Operculum_OP8_L	.5560	2.21	.0271
		Julich-Brain	Premotor_6D2_L	.6601	2.45	.0142
	FRONTAL_R	AAL3	N_Acc_R	.6172	2.22	.0262
		Julich-Brain	GapMap_FRONTAL-TO-OCCIPITAL_R	.5029	2.03	.0420
		Julich-Brain	GapMap_FRONTAL-TO-TEMPORAL-II_R	.5445	2.20	.0280
		Julich-Brain	OFC_FO6_R	.5082	1.99	.0462
		Julich-Brain	Operculum_OP8_R	.5065	2.04	.0416
	TEMPORAL_L	Julich-Brain	Hippocampus_DG_L	.4933	1.99	.0471
		Julich-Brain	Hippocampus_SUB_L	.5302	2.08	.0379
		Julich-Brain	Parahippocampal_PH1_L	.4736	2.00	.0457
	TEMPORAL_R	–	TEMPORAL_R	.4958	2.01	.0441
		Julich-Brain	Amygdala_SF_R	.5110	2.03	.0421
		Julich-Brain	GapMap_TEMPORAL-TO-PARIETAL_R	.5741	2.22	.0267
		Julich-Brain	Hippocampus_EC_R	.7510	2.74	.0061
		Julich-Brain	Hippocampus_SUB_R	.5602	2.21	.0270
		Julich-Brain	Hippocampus_TRS_R	.7421	2.52	.0117
		Julich-Brain	Parahippocampal_PH3_R	.6664	2.45	.0142
	THALAMUS_L	AAL3	Thal_MDm_L	.5392	2.07	.0384
		AAL3	Thal_VPL_L	.5222	2.04	.0416
	THALAMUS_R	AAL3	Thal_LGN_R	.5213	1.98	.0481
		AAL3	Thal_VA_R	.5658	2.06	.0390
PDQ-39	CEREBELLUM_L	AAL3	Cerebellum_8_L	.6884	2.33	.0200
		AAL3	Vermis_6	−.6921	−2.15	.0314
		Julich-Brain	Cerebellum_NFAST_L	.6508	2.06	.0395
	CEREBELLUM_R	Julich-Brain	Cerebellum_NDENTD_R	.6027	2.20	.0280
	CINGULATE_GYRUS_L	Julich-Brain	Cingulum_25_L	−.7529	−2.35	.0189
	CINGULATE_GYRUS_R	–	CINGULATE_GYRUS_R	−.6399	−2.06	.0393
		Julich-Brain	Cingulum_25_R	−.7411	−2.36	.0182
		Julich-Brain	Cingulum_33_R	−.5844	−2.02	.0438
	FRONTAL_L	Julich-Brain	GapMap_FRONTAL-II_L	−.6485	−2.15	.0318
		Julich-Brain	Premotor_6D2_L	−.7480	−2.46	.0137
		Julich-Brain	PRESMA_L	−.6074	−2.09	.0364
	FRONTAL_R	AAL3	N_Acc_R	−.7982	−2.49	.0127
		Julich-Brain	Bforebrain_4_R	−.5786	−1.98	.0483
		Julich-Brain	GapMap_FRONTAL-TO-TEMPORAL-I_R	−.5476	−1.97	.0483
		Julich-Brain	Operculum_OP5_R	−.5583	−2.01	.0441
		Julich-Brain	Premotor_6D2_R	−.7024	−2.36	.0182
		Julich-Brain	SFG_8D1_R	−.5625	−1.97	.0490
	PARIETAL_L	Julich-Brain	IPL_PFOP_L	−.5659	−2.07	.0383
	TEMPORAL_L	Julich-Brain	Amygdala_CM_L	−.7491	−2.15	.0312
	TEMPORAL_R	Julich-Brain	Hippocampus_EC_R	−.7058	−2.40	.0166
		Julich-Brain	Hippocampus_SUB_R	−.5340	−1.99	.0467
		Julich-Brain	Hippocampus_TRS_R	−.6079	−2.01	.0449
		Julich-Brain	Parahippocampal_PH3_R	−.7192	−2.37	.0178
UPDRS-3	CEREBELLUM_L	AAL3	Cerebellum_4_5_L	−.5650	−1.97	.0492
	CEREBELLUM_R	Julich-Brain	Cerebellum_NFAST_R	−.6563	−2.06	.0393
	TEMPORAL_L	Julich-Brain	Hippocampus_TRS_L	−.6044	−2.25	.0242
	TEMPORAL_R	Julich-Brain	Amygdala_SF_R	−.5365	−2.06	.0398
		Julich-Brain	Hippocampus_EC_R	−.4998	−2.02	.0437
	THALAMUS_L	AAL3	Thal_MDl_L	−.6064	−2.10	.0361
		AAL3	Thal_MDm_L	−.6183	−2.34	.0190
	THALAMUS_R	AAL3	Thal_LGN_R	−.5838	−2.04	.0413
		AAL3	Thal_MDl_R	−.5337	−1.97	.0485

Further associations were found with orbitofrontal and inferior frontal areas FO5/6 and OP8 (Wojtasik et al., 2020). Some of these regions showed also pronounced group differences. The thalamic nuclei MD, VPL, VA and LGN were also associated with MMSE changes. The small longitudinal changes in MMSE of most of the patients could be considered as a disadvantage for this association analysis, but on the other hand, this suggests that our results were not influenced by potential

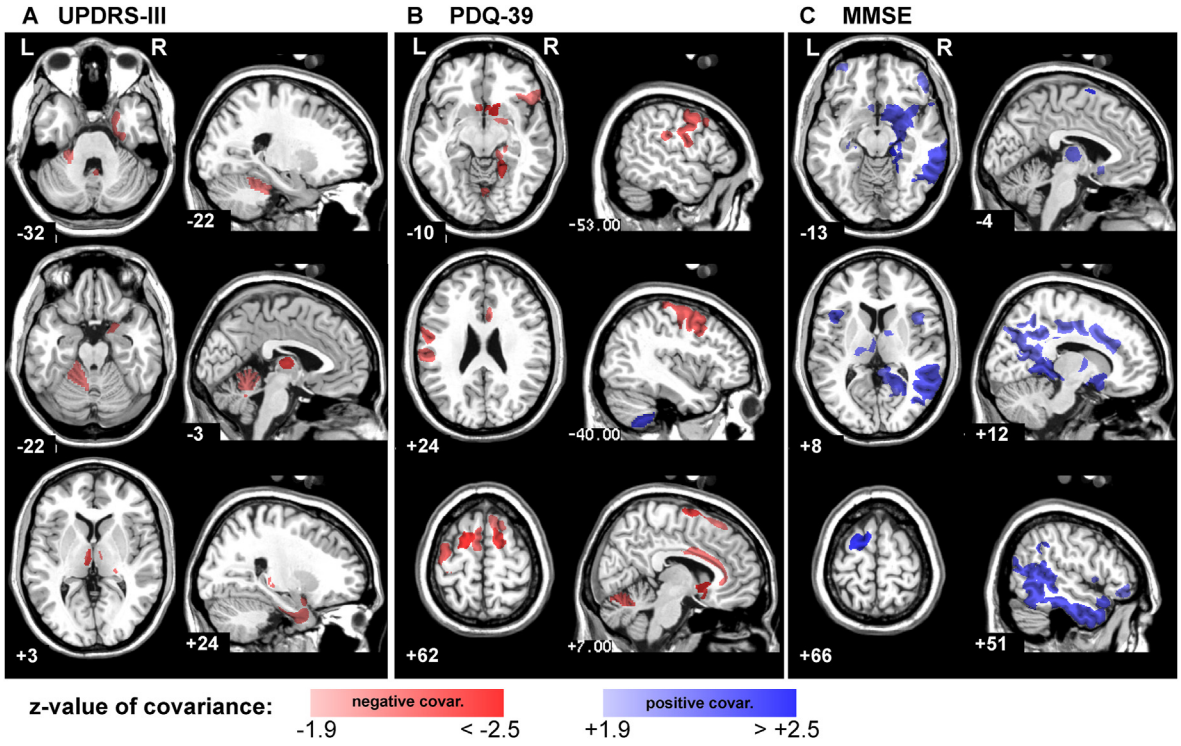

Fig. 6 – Longitudinal associations of clinical scores with regional volume changes in PD patients. (A) Associations of changes of region volumes with changes of UPDRS-III score (motor examinations). Regions with significant negative associations are colored in red, and positive associations in blue. (B) Associations with changes of PDQ-39. (C) Associations with changes of MMSE.

additional (undiscovered) neurodegenerative diseases (e.g., Alzheimer's disease) of the present patient cohort. One reason for these relatively small changes of MMSE could be that the patient sample was relatively young (mean baseline age 53.2 years) in comparison with other studies, (e.g., Filippi et al., 2020; Gorges et al., 2020; Mak et al., 2015).

The PDQ-39 showed in the baseline analysis negative associations mainly with the volumes of regions in the frontal cortex, e.g., inferior frontal areas 44/45, OP6/8/9, orbitofrontal area FO3 (Henssen et al., 2016; Wojtasik et al., 2020), frontal pole area FP1 (Bludau et al., 2014), and dorsal premotor areas 6D2/3. Further associations were found with parietal and occipital areas, mainly in the left hemisphere. The longitudinal changes of the PDQ-39 were negatively associated mainly with areas of the dorsal frontal cortex (6D2, PreSMA, 8D1), but also with the nucleus accumbens and nucleus basalis Meynert in the basal forebrain, with cingulate areas 25 and 33, and regions in the medial temporal lobe (left amygdala nucleus CM, right entorhinal cortex, subiculum, area PH3). The PDQ-39 score summarizes a broad range of impairments in PD including motor control, emotional well-being, and social behavior. All these functions rely on frontal-executive functions. Moreover, a strong association of the PDQ-39 with apathy was reported (Barone et al., 2009), and apathy or depression, which frequently occur in PD, had been shown to be associated with damages of prefrontal and cingulate regions (Benoit & Robert, 2011; Pagonabarraga, Kulisevsky, Strafella, & Krack, 2015).

Several studies of brain structure with rather large samples of PD patients and controls had been conducted in the past years. Three studies analyzed longitudinally cortical thickness and regional volumes of PD patients (Filippi et al., 2020; Gorges et al., 2020; Mak et al., 2015): The baseline data of these studies suggested concordantly that in PD patients temporoparietal and dorsolateral frontal regions were atrophied in comparison with controls. These differences were particularly pronounced in patients with cognitive impairments. The longitudinal findings, however, differed between the three studies: Early stage PD patients with mild cognitive impairment (MCI) showed also longitudinally accelerated atrophy in the abovementioned regions (Mak et al., 2015), whereas PD patients in a later stage with MCI showed less atrophic changes than cognitively normal patients (Filippi et al., 2020), and PD patients in advanced stage (mean disease duration 8.9 years) showed a global atrophy rate similar to the age-related atrophy in controls (Gorges et al., 2020). These findings suggest that atrophy caused by PD seems to reach a plateau in later stages, and in patients with cognitive impairments this process seems to be pushed forward. The present study examined less patients but with more time points than the aforementioned studies, and most of them were in a rather early stage (mean disease duration 3.7 years). The group comparison of patients and controls yielded a pattern of accelerated longitudinal atrophy in patients in temporal, parietal, inferior frontal cortices and basal ganglia which agrees with the atrophic changes of early-stage patients found in the

aforementioned studies, apart from the absence of changes in the dorsal frontal cortex. Interestingly, the baseline comparison of advanced-stage patients in Gorges et al. (2020) and the longitudinal results of the present study indicate concordantly, that mainly gray matter is affected by atrophy in PD. The grouping of patients in the present study by their cognitive changes also disclosed several cortical regions, where atrophy was stronger in patients with cognitive decline in comparison with cognitively more stable patients (Supplemental Fig. 4). These group differences in regional atrophy rates show similarities with the previously mentioned studies, however, they do not match with the bivariate LMM analysis (Fig. 6), which may be caused by the limitations of cognitive state estimation by the MMSE alone (see below). These findings are more thoroughly discussed in chapter "Cognitive changes in PD patients" in the Supplemental material.

The PPMI database (www.ppmi-info.org) (Marek et al., 2018) provides comprehensive longitudinal multimodal imaging, clinical and genetic data of PD patients and controls, which had been analyzed in several studies. A recent longitudinal DBM study yielded accelerated atrophy in the caudate and accumbens nuclei, hippocampus and regions of temporal, parietal and occipital cortices (Tremblay et al., 2021), which agreed well with the present study. Zeighami et al. analyzed the baseline MR images of the PPMI database by DBM in order to identify atrophy patterns and relate them with clinical variables (Zeighami et al., 2015, 2019). An independent-component analysis of DBM data yielded a pattern encompassing basal ganglia, basal forebrain, mesencephalon, pons, and several cortical regions (Zeighami et al., 2015), which was correlated with the UPDRS-III score, and which also resembled different connectivity based networks. A comprehensive multivariate analysis of clinical variables and DBM maps yielded a similar atrophy pattern that was associated with both, motor and cognitive scores (Zeighami et al., 2019). This pattern encompassed basal ganglia, basal forebrain and mainly temporal, occipital and inferior frontal regions, similar to the findings of the present study, apart from atrophy found in dorsolateral frontal regions.

5. Strengths and limitations

A major strength of the present study results from the long observation periods and large number of observations of each subject (up to 8.8 years). This enables in some subjects detailed visualizations of atrophy progression as in Fig. 5. For the analysis of structural changes a DBM implementation was used that is optimized for longitudinal analyses, because structural changes are detected by intra-subject registrations of follow-up images with the baseline image, whereas other DBM implementations apply a inter-subject registration with a common reference image. For the definitions of anatomical regions, we used the Julich-Brain atlas, which encompasses cytoarchitectonic areas and nuclei. This atlas reflects the microanatomical structure of the brain while taking into account the inter-subject variability. Finally, the longitudinal data were analyzed by linear mixed models, which have the advantage, that the data of all time points can be analyzed in one step, instead of separate analyses of each time point. Moreover, they account for differences in time points (or intervals), and numbers of measurements, i.e., they are more flexible than e.g., repeated measures ANOVA models.

There are also some limitations: First, the number of subjects is limited in comparison with other recent studies, which may influence the generalizability in particular of the baseline group comparison and correlation analyses, but also the longitudinal analyses, even though the later benefit from the large number of follow-up time points per subject. Second, the cognitive status of the subjects was examined only by the MMSE. This might have impeded more sensitive analyses of associations between cognition and atrophic changes. Previous studies found atrophy differences between cognitively stable PD patients and those with mild cognitive impairment (MCI). Such a distinction was only approximately possible in the present study (Supplemental material, Section 5). Third, the MR images of this study had been acquired on two different scanners, which could have an influence on the calculation of region volumes. However, the images of each series (i.e., of each subject) had been acquired on one and the same scanner. Therefore it can be assumed that the scanner had only a minor impact on the longitudinal analyses.

6. Conclusions

Based on maps of microstructurally defined brain regions, longitudinal DBM revealed in-vivo a detailed, characteristic spatio-temporal pattern of atrophy in patients with PD, which seems to reflect the propagation of αSyn-aggregates in the brain as demonstrated in neuropathological studies (Braak et al., 2006).

Data availability and transparency statement

We report how we determined our sample size, all data exclusions, all inclusion/exclusion criteria, whether inclusion/exclusion criteria were established prior to data acquisition, all manipulations, and all measures in the study. No part of these procedures was pre-registered prior to this study. The SAS-scripts used for the statistical analysis are stored in a public repository (https://doi.org/10.26165/JUELICH-DATA/YYXPBF). The ethics approval of this study does not permit the sharing of any MR images or clinical examination data, or their storage in publicly accessible repositories.

Funding

This work received support by the European Union's Horizon 2020 Framework Programme for Research and Innovation under Grant Agreement No. 785907 (Human Brain Project SGA2) and Grant Agreement No. 945539 (Human Brain Project SGA3).

Author contributions

Peter Pieperhoff: Methodology, Software, Writing-Original Draft, Visualization. **Martin Südmeyer:** Conceptualization, Investigation, Resources, Writing-Review&Editing, Project administration. **Lars Dinkelbach:** Investigation, Writing-Review&Editing. **Christian J. Hartmann:** Investigation, Writing-Review&Editing. Stefano Ferrea: Investigation, Writing-Review&Editing. **Alexia S. Moldovan:** Investigation, Writing-Review&Editing. **Martina Minnerop:** Investigation, Writing-Review&Editing. **Sandra Diaz-Pier:** Software, Writing-Review&Editing. **Alfons Schnitzler:** Conceptualization, Writing-Review&Editing, Resources, Supervision, Funding acquisition. **Katrin Amunts:** Conceptualization, Writing-Review&Editing, Resources, Supervision, Funding acquisition.

Acknowledgments

The authors thank the reviewers for comments and suggestions which helped to improve this article. The JURECA computer cluster (Krause & Thörnig, 2016) in the Research Centre Jülich was used for all image registrations. Therefore, the authors gratefully acknowledge the computing time granted by the JARA-HPC Vergabegremium on the supercomputer JURECA at Forschungszentrum Jülich. They thank Heiko Braak and Kelly Del-Tredici Braak for inspiring discussion.

Declaration of competing interest

The authors have no conflict of interest to declare.

Supplementary data

Supplementary data to this article can be found online at https://doi.org/10.1016/j.cortex.2022.03.009.

REFERENCES

Aggleton, J. P. (2012). Multiple anatomical systems embedded within the primate medial temporal lobe: Implications for hippocampal function. *Neuroscience and Biobehavioral Reviews, 36*(7), 1579–1596. https://doi.org/10.1016/j.neubiorev.2011.09.005

Amunts, K., Kedo, O., Kindler, M., Pieperhoff, P., Mohlberg, H., Shah, N. J., et al. (2005). Cytoarchitectonic mapping of the human amygdala, hippocampal region and entorhinal cortex: Intersubject variability and probability maps. *Anatomy and Embryology, 210*(5–6), 343–352. https://doi.org/10.1007/s00429-005-0025-5

Amunts, K., Malikovic, A., Mohlberg, H., Schormann, T., & Zilles, K. (2000). Brodmann's areas 17 and 18 brought into stereotaxic space-where and how variable? *NeuroImage, 11*(1), 66–84.

Amunts, K., Mohlberg, H., Bludau, S., & Zilles, K. (2020). Julich-brain: A 3D probabilistic atlas of the human brain's cytoarchitecture. *Science, 369*(6506), 988–992. https://doi.org/10.1126/science.abb4588

Amunts, K., Schleicher, A., Bürgel, U., Mohlberg, H., Uylings, H. B., & Zilles, K. (1999). Broca's region revisited: Cytoarchitecture and intersubject variability. *Journal of Comparative Neurology, 412*(2), 319–341.

Amunts, K., & Zilles, K. (2015). Architectonic mapping of the human brain beyond Brodmann. *Neuron, 88*(6), 1086–1107. https://doi.org/10.1016/j.neuron.2015.12.001

Ashburner, J., & Friston, K. J. (2005). Unified segmentation. *NeuroImage, 26*(3), 839–851. https://doi.org/10.1016/j.neuroimage.2005.02.018

Aubert-Broche, B., Evans, A. C., & Collins, L. (2006). A new improved version of the realistic digital brain phantom. *NeuroImage, 32*(1), 138–145. https://doi.org/10.1016/j.neuroimage.2006.03.052

Barone, P., Antonini, A., Colosimo, C., Marconi, R., Morgante, L., Avarello, T. P., et al. (2009). The PRIAMO study: A multicenter assessment of nonmotor symptoms and their impact on quality of life in Parkinson's disease. *Movement Disorders, 24*(11), 1641–1649. https://doi.org/10.1002/mds.22643

Benjamini, Y., & Bogomolov, M. (2014). Selective inference on multiple families of hypotheses. *Journal of the Royal Statistical Society: Series B (Statistical Methodology), 76*(1), 297–318. https://doi.org/10.1111/rssb.12028

Benjamini, Y., & Hochberg, Y. (1995). Controlling the false discovery rate: A practical and powerful approach to multiple testing. *Journal of the Royal Statistical Society: Series B (Methodological), 57*(1), 289–300. https://doi.org/10.1111/j.2517-6161.1995.tb02031.x

Benoit, M., & Robert, P. H. (2011). Imaging correlates of apathy and depression in Parkinson's disease. *Journal of the Neurological Sciences, 310*(1), 58–60. https://doi.org/10.1016/j.jns.2011.07.006

Beyer, M. K., Janvin, C. C., Larsen, J. P., & Aarsland, D. (2007). A magnetic resonance imaging study of patients with Parkinson's disease with mild cognitive impairment and dementia using voxel-based morphometry. *J Neurol Neurosurg Psychiatry, 78*(3), 254–259.

Bludau, S., Eickhoff, S. B., Mohlberg, H., Caspers, S., Laird, A. R., Fox, P. T., et al. (2014). Cytoarchitecture, probability maps and functions of the human frontal pole. *NeuroImage, 93*, 260–275. https://doi.org/10.1016/j.neuroimage.2013.05.052

Borroni, B., Premi, E., Formenti, A., Turrone, R., Alberici, A., Cottini, E., et al. (2015). Structural and functional imaging study in dementia with Lewy bodies and Parkinson's disease dementia. *Parkinsonism & Related Disorders, 21*(9), 1049–1055.

Braak, H., Bohl, J. R., Müller, C. M., Rüb, U., de Vos, R. A. I., & Del Tredici, K. (2006). Stanley Fahn Lecture 2005: The staging procedure for the inclusion body pathology associated with sporadic Parkinson's disease reconsidered. *Movement Disorders: Official Journal of the Movement Disorder Society, 21*(12), 2042–2051.

Braak, H., Del Tredici, K., Rüb, U., de Vos, R. A. I., Jansen Steur, E. N. H., & Braak, E. (2003). Staging of brain pathology related to sporadic Parkinson's disease. *Neurobiology of Aging, 24*(2), 197–211.

Braak, H., Rüb, U., Jansen Steur, E. N. H., Del Tredici, K., & de Vos, R. A. I. (2005). Cognitive status correlates with neuropathologic stage in Parkinson disease. *Neurology, 64*(8), 1404–1410.

Brooks, D. J., & Tambasco, N. (2016). Imaging synucleinopathies. *Movement Disorders: Official Journal of the Movement Disorder Society, 31*(6), 814–829. https://doi.org/10.1002/mds.26547

Burton, E. J., McKeith, I. G., Burn, D. J., & O'Brien, J. T. (2005). Brain atrophy rates in Parkinson's disease with and without dementia using serial magnetic resonance imaging. *Movement Disorders: Official Journal of the Movement Disorder Society, 20*(12), 1571–1576.

Burton, E. J., McKeith, I. G., Burn, D. J., Williams, E. D., & O'Brien, J. T. (2004). Cerebral atrophy in Parkinson's disease

with and without dementia: A comparison with Alzheimer's disease, dementia with Lewy bodies and controls. *Brain, 127*(Pt 4), 791–800.
Caspers, S., Eickhoff, S. B., Geyer, S., Scheperjans, F., Mohlberg, H., Zilles, K., et al. (2008). The human inferior parietal lobule in stereotaxic space [journal article] *Brain Structure & Function, 212*(6), 481–495. https://doi.org/10.1007/s00429-008-0195-z.
Caspers, J., Zilles, K., Eickhoff, S. B., Schleicher, A., Mohlberg, H., & Amunts, K. (2013). Cytoarchitectonical analysis and probabilistic mapping of two extrastriate areas of the human posterior fusiform gyrus [journal article] *Brain Structure & Function, 218*(2), 511–526. https://doi.org/10.1007/s00429-012-0411-8.
De Groote, E., De Keyser, K., Bockstael, A., Botteldooren, D., Santens, P., & De Letter, M. (2020). Central auditory processing in parkinsonian disorders: A systematic review. *Neuroscience and Biobehavioral Reviews, 113*, 111–132. https://doi.org/10.1016/j.neubiorev.2020.03.001
Ding, S. L. (2013). Comparative anatomy of the prosubiculum, subiculum, presubiculum, postsubiculum, and parasubiculum in human, monkey, and rodent. *Journal of Comparative Neurology, 521*(18), 4145–4162. https://doi.org/10.1002/cne.23416
Duncan, G. W., Firbank, M. J., Yarnall, A. J., Khoo, T. K., Brooks, D. J., Barker, R. A., et al. (2016). Gray and white matter imaging: A biomarker for cognitive impairment in early Parkinson's disease? *Movement Disorders: Official Journal of the Movement Disorder Society, 31*(1), 103–110.
Fearnley, J. M., & Lees, A. J. (1991). Ageing and Parkinson's disease: Substantia nigra regional SELECTIVITY. *Brain, 114*(5), 2283–2301. https://doi.org/10.1093/brain/114.5.2283
Filippi, M., Canu, E., Donzuso, G., Stojkovic, T., Basaia, S., Stankovic, I., et al. (2020). Tracking cortical changes throughout cognitive decline in Parkinson's disease. *Movement Disorders, 35*(11), 1987–1998. https://doi.org/10.1002/mds.28228
Folstein, M. F., Folstein, S. E., & McHugh, P. R. (1975). "Mini-mental state": A practical method for grading the cognitive state of patients for the clinician. *Journal of Psychiatric Research, 12*(3), 189–198. https://doi.org/10.1016/0022-3956(75)90026-6
Forno, L. S. (1996). Neuropathology of Parkinson's disease. *Journal of Neuropathology and Experimental Neurology, 55*(3), 259–272.
Gee, M., Dukart, J., Draganski, B., Wayne Martin, W. R., Emery, D., & Camicioli, R. (2017). Regional volumetric change in Parkinson's disease with cognitive decline. *Journal of the Neurological Sciences, 373*, 88–94.
Goetz, C. G., Tilley, B. C., Shaftman, S. R., Stebbins, G. T., Fahn, S., Martinez-Martin, P., et al. (2008). Movement disorder society-sponsored revision of the unified Parkinson's disease rating Scale (MDS-UPDRS): Scale presentation and clinimetric testing results. *Movement Disorders: Official Journal of the Movement Disorder Society, 23*(15), 2129–2170.
Gorges, M., Kunz, M. S., Müller, H.-P., Liepelt-Scarfone, I., Storch, A., Dodel, R., et al. (2020). Longitudinal brain atrophy distribution in advanced Parkinson's disease: What makes the difference in "cognitive status" converters? *Human Brain Mapping, 41*(6), 1416–1434. https://doi.org/10.1002/hbm.24884
Hawkes, C. H., Del Tredici, K., & Braak, H. (2010). A timeline for Parkinson's disease. *Parkinsonism & Related Disorders, 16*(2), 79–84.
Henn, S. (2003). A Levenberg-Marquardt scheme for nonlinear image registration. *BIT Numerical Mathematics, 43*(4), 743–759.
Henssen, A., Zilles, K., Palomero-Gallagher, N., Schleicher, A., Mohlberg, H., Gerboga, F., et al. (2016). Cytoarchitecture and probability maps of the human medial orbitofrontal cortex. *Cortex, 75*, 87–112. https://doi.org/10.1016/j.cortex.2015.11.006
Holmes, C. J., Hoge, R., Collins, L., Woods, R., Toga, A. W., & Evans, A. C. (1998). Enhancement of MR images using registration for signal averaging. *Journal of Computer Assisted Tomography, 22*(2), 324–333.
Jafari, Z., Kolb, B. E., & Mohajerani, M. H. (2020). Auditory dysfunction in Parkinson's disease. *Movement Disorders, 35*(4), 537–550. https://doi.org/10.1002/mds.28000
Jenkinson, M., & Smith, S. (2001). A global optimisation method for robust affine registration of brain images. *Medical Image Analysis, 5*(2), 143–156. https://doi.org/10.1016/S1361-8415(01)00036-6
Kaasinen, V., Vahlberg, T., Stoessl, A. J., Strafella, A. P., & Antonini, A. (2021). Dopamine receptors in Parkinson's disease: A meta-analysis of imaging studies. *Movement Disorders*. https://doi.org/10.1002/mds.28632. n/a(n/a).
Krause, D., & Thörnig, P. (2016). JURECA: General-purpose supercomputer at Jülich supercomputing centre. *Journal of Large-scale Research Facilities, 2*(A62). https://doi.org/10.17815/jlsrf-2-121
Kujovic, M., Zilles, K., Malikovic, A., Schleicher, A., Mohlberg, H., Rottschy, C., et al. (2013). Cytoarchitectonic mapping of the human dorsal extrastriate cortex. *Brain Structure & Function, 218*(1), 157–172. https://doi.org/10.1007/s00429-012-0390-9 [journal article].
Kurita, A., Koshikawa, H., Akiba, T., Seki, K., Ishikawa, H., & Suzuki, M. (2019). Visual hallucinations and impaired conscious visual perception in Parkinson disease. *Journal of Geriatric Psychiatry and Neurology, 33*(6), 377–385. https://doi.org/10.1177/0891988719892318
Lech, R. K., & Suchan, B. (2013). The medial temporal lobe: Memory and beyond. *Behavioural Brain Research, 254*, 45–49. https://doi.org/10.1016/j.bbr.2013.06.009
Lee, H. M., Kwon, K.-Y., Kim, M.-J., Jang, J.-W., Suh, S.-I., Koh, S.-B., et al. (2014). Subcortical grey matter changes in untreated, early stage Parkinson's disease without dementia. *Parkinsonism & Related Disorders, 20*(6), 622–626.
Leow, A. D., Yanovsky, I., Chiang, M. C., Lee, A. D., Klunder, A. D., Lu, A., et al. (2007). Statistical properties of Jacobian maps and the realization of unbiased large-deformation nonlinear image registration. *IEEE Transactions on Medical Imaging, 26*(6), 822–832. https://doi.org/10.1109/tmi.2007.892646
Lewis, M. M., Smith, A. B., Styner, M., Gu, H., Poole, R., Zhu, H., et al. (2009). Asymmetrical lateral ventricular enlargement in Parkinson's disease. *European Journal of Neurology: the Official Journal of the European Federation of Neurological Societies, 16*(4), 475–481.
Lewy, F. H. (1912). Paralysis agitans. I. Pathologische anatomie [Book chapter]. In M. Lewandowsky (Ed.). *Handbuch der neurologie* (Vol. 3/11, pp. 920–933). Berlin: Julius Springer.
Lorenz, S., Weiner, K. S., Caspers, J., Mohlberg, H., Bludau, S., Schleicher, A., et al. (2015). Two new cytoarchitectonic areas on the human mid-fusiform gyrus. *Cerebral Cortex, 27*(1), 373–385. https://doi.org/10.1093/cercor/bhv225
Mak, E., Su, L., Williams, G. B., Firbank, M. J., Lawson, R. A., Yarnall, A. J., et al. (2015). Baseline and longitudinal grey matter changes in newly diagnosed Parkinson's disease: ICICLE-PD study. *Brain, 138*(10), 2974.
Malikovic, A., Amunts, K., Schleicher, A., Mohlberg, H., Eickhoff, S. B., Wilms, M., et al. (2007). Cytoarchitectonic analysis of the human extrastriate cortex in the region of V5/MT+: A probabilistic, stereotaxic map of area hOc5. *Cerebral Cortex, 17*(3), 562–574. https://doi.org/10.1093/cercor/bhj181
Malikovic, A., Amunts, K., Schleicher, A., Mohlberg, H., Kujovic, M., Palomero-Gallagher, N., et al. (2016). Cytoarchitecture of the human lateral occipital cortex: Mapping of two extrastriate areas hOc4la and hOc4lp. *Brain Structure & Function, 221*(4), 1877–1897. https://doi.org/10.1007/s00429-015-1009-8 [journal article].
Marek, K., Chowdhury, S., Siderowf, A., Lasch, S., Coffey, C. S., Caspell-Garcia, C., & the Parkinson's Progression Markers, I.

(2018). The Parkinson's progression markers initiative (PPMI) – establishing a PD biomarker cohort. *Annals of Clinical and Translational Neurology, 5*(12), 1460–1477. https://doi.org/10.1002/acn3.644

Menke, R. A. L., Szewczyk-Krolikowski, K., Jbabdi, S., Jenkinson, M., Talbot, K., Mackay, C. E., et al. (2014). Comprehensive morphometry of subcortical grey matter structures in early-stage Parkinson's disease. *Human Brain Mapping, 35*(4), 1681–1690.

Modersitzki, J. (2003). *Numerical methods for image registration*. Oxford: Oxford University Press.

Morosan, P., Rademacher, J., Schleicher, A., Amunts, K., Schormann, T., & Zilles, K. (2001). Human primary auditory cortex: Cytoarchitectonic subdivisions and mapping into a spatial reference system. *NeuroImage, 13*(4), 684–701. https://doi.org/10.1006/nimg.2000.0715

Pagonabarraga, J., Kulisevsky, J., Strafella, A. P., & Krack, P. (2015). Apathy in Parkinson's disease: Clinical features, neural substrates, diagnosis, and treatment. *The Lancet Neurology, 14*(5), 518–531. https://doi.org/10.1016/S1474-4422(15)00019-8

Palomero-Gallagher, N., Eickhoff, S. B., Hoffstaedter, F., Schleicher, A., Mohlberg, H., Vogt, B. A., et al. (2015). Functional organization of human subgenual cortical areas: Relationship between architectonical segregation and connectional heterogeneity. *NeuroImage, 115*, 177–190. https://doi.org/10.1016/j.neuroimage.2015.04.053

Palomero-Gallagher, N., Kedo, O., Mohlberg, H., Zilles, K., & Amunts, K. (2020). Multimodal mapping and analysis of the cyto- and receptorarchitecture of the human hippocampus. *Brain Structure & Function, 225*(3), 881–907. https://doi.org/10.1007/s00429-019-02022-4

Parkkinen, L., Kauppinen, T., Pirttilä, T., Autere, J. M., & Alafuzoff, I. (2005). Alpha-synuclein pathology does not predict extrapyramidal symptoms or dementia. *Annals of Neurology, 57*(1), 82–91.

Parkkinen, L., Pirttilä, T., & Alafuzoff, I. (2008). Applicability of current staging/categorization of alpha-synuclein pathology and their clinical relevance. *Acta Neuropathologica, 115*(4), 399–407.

Park, A., & Stacy, M. (2009). Non-motor symptoms in Parkinson's disease. *Journal of Neurology, 256*(3), 293–298. https://doi.org/10.1007/s00415-009-5240-1

Pereira, J. B., Ibarretxe-Bilbao, N., Marti, M.-J., Compta, Y., Junqué, C., Bargallo, N., et al. (2012). Assessment of cortical degeneration in patients with Parkinson's disease by voxel-based morphometry, cortical folding, and cortical thickness. *Human Brain Mapping, 33*(11), 2521–2534.

Pereira, J. B., Svenningsson, P., Weintraub, D., Bronnick, K., Lebedev, A., Westman, E., et al. (2014). Initial cognitive decline is associated with cortical thinning in early Parkinson disease. *Neurology, 82*(22), 2017–2025. https://doi.org/10.1212/wnl.0000000000000483

Peterson, D. S., & Horak, F. B. (2016). Neural control of walking in people with parkinsonism. *Physiology, 31*(2), 95–107. https://doi.org/10.1152/physiol.00034.2015

Peto, V., Jenkinson, C., Fitzpatrick, R., & Greenhall, R. (1995). The development and validation of a short measure of functioning and well being for individuals with Parkinson's disease. *Quality of Life Research: an International Journal of Quality of Life Aspects of Treatment, Care and Rehabilitation, 4*(3), 241–248.

Pieperhoff, P., Südmeyer, M., Hömke, L., Zilles, K., Schnitzler, A., & Amunts, K. (2008). Detection of structural changes of the human brain in longitudinally acquired MR images by deformation field morphometry: Methodological analysis, validation and application. *Neuroimage, 43*(2), 269–287.

Planetta, P. J., Kurani, A. S., Shukla, P., Prodoehl, J., Corcos, D. M., Comella, C. L., et al. (2015). Distinct functional and macrostructural brain changes in Parkinson's disease and multiple system atrophy. *Human Brain Mapping, 36*(3), 1165–1179.

Polymeropoulos, M. H., Lavedan, C., Leroy, E., Ide, S. E., Dehejia, A., Dutra, A., et al. (1997). Mutation in the alpha-synuclein gene identified in families with Parkinson's disease. *Science, 276*(5321), 2045–2047.

Ramírez-Ruiz, B., Martí, M. J., Tolosa, E., Bartrés-Faz, D., Summerfield, C., Salgado-Pineda, P., et al. (2005). Longitudinal evaluation of cerebral morphological changes in Parkinson's disease with and without dementia. *Journal of Neurology, 252*(11), 1345–1352.

Rolls, E. T., Huang, C.-C., Lin, C.-P., Feng, J., & Joliot, M. (2020). Automated anatomical labelling atlas 3. *NeuroImage, 206*, 116189. https://doi.org/10.1016/j.neuroimage.2019.116189

Rottschy, C., Eickhoff, S. B., Schleicher, A., Mohlberg, H., Kujovic, M., Zilles, K., et al. (2007). Ventral visual cortex in humans: Cytoarchitectonic mapping of two extrastriate areas. *Human Brain Mapping, 28*(10), 1045–1059. https://doi.org/10.1002/hbm.20348

Scheperjans, F., Eickhoff, S. B., Hömke, L., Mohlberg, H., Hermann, K., Amunts, K., et al. (2008). Probabilistic maps, morphometry, and variability of cytoarchitectonic areas in the human superior parietal cortex. *Cerebral Cortex, 18*(9), 2141–2157. https://doi.org/10.1093/cercor/bhm241

Simes, R. J. (1986). An improved Bonferroni procedure for multiple tests of significance. *Biometrika, 73*(3), 751–754. https://doi.org/10.1093/biomet/73.3.751

Spillantini, M. G., Schmidt, M. L., Lee, V. M., Trojanowski, J. Q., Jakes, R., & Goedert, M. (1997). Alpha-synuclein in Lewy bodies. *Nature, 388*(6645), 839–840. https://doi.org/10.1038/42166

Studholme, C., Drapaca, C., Iordanova, B., & Cardenas, V. (2006). Deformation-based mapping of volume change from serial brain MRI in the presence of local tissue contrast change. *IEEE Transactions on Medical Imaging, 25*(5), 626–639. https://doi.org/10.1109/TMI.2006.872745

Südmeyer, M., Pieperhoff, P., Ferrea, S., Krause, H., Groiss, S. J., Elben, S., et al. (2012). Longitudinal deformation-based morphometry reveals spatio-temporal dynamics of brain volume changes in patients with corticobasal syndrome. *Plos One, 7*(7), Article e41873. https://doi.org/10.1371/journal.pone.0041873

Summerfield, C., Junqué, C., Tolosa, E., Salgado-Pineda, P., Gómez-Ansón, B., Martí, M. J., et al. (2005). Structural brain changes in Parkinson disease with dementia: A voxel-based morphometry study. *Archives of Neurology, 62*(2), 281–285.

Thiébaut, R., Jacqmin-Gadda, H., Chêne, G., Leport, C., & Commenges, D. (2002). Bivariate linear mixed models using SAS proc MIXED. *Computer Methods and Programs in Biomedicine, 69*(3), 249–256.

Tremblay, C., Rahayel, S., Vo, A., Morys, F., Shafiei, G., Abbasi, N., et al. (2021). Brain atrophy progression in Parkinson's disease is shaped by connectivity and local vulnerability. *Brain Communications, 3*(4). https://doi.org/10.1093/braincomms/fcab269

Tustison, N. J., Avants, B. B., Cook, P. A., Zheng, Y., Egan, A., Yushkevich, P. A., et al. (2010). N4ITK: Improved N3 bias correction. *IEEE Transactions on Medical Imaging, 29*(6), 1310–1320. https://doi.org/10.1109/TMI.2010.2046908

Tzourio-Mazoyer, N., Landeau, B., Papathanassiou, D., Crivello, F., Etard, O., Delcroix, N., et al. (2002). Automated anatomical labeling of activations in SPM using a macroscopic anatomical parcellation of the MNI MRI single-subject brain. *NeuroImage, 15*(1), 273–289.

Verbeke, G., & Molenberghs, G. (2000). *Linear mixed models for longitudinal data*. New York: Springer-Verlag.

Weil, R. S., Schrag, A. E., Warren, J. D., Crutch, S. J., Lees, A. J., & Morris, H. R. (2016). Visual dysfunction in Parkinson's disease.

Brain, 139(11), 2827–2843. https://doi.org/10.1093/brain/aww175

Wenning, G. K., Colosimo, C., Geser, F., & Poewe, W. (2004). Multiple system atrophy. *The Lancet Neurology, 3*(2), 93–103. https://doi.org/10.1016/S1474-4422(03)00662-8

Wenning, G. K., Tison, F., Elliott, L., Quinn, N. P., & Daniel, S. E. (1996). Olivopontocerebellar pathology in multiple system atrophy. *Movement Disorders: Official Journal of the Movement Disorder Society, 11*(2), 157–162. https://doi.org/10.1002/mds.870110207

Wojtasik, M., Bludau, S., Eickhoff, S. B., Mohlberg, H., Gerboga, F., Caspers, S., et al. (2020). Cytoarchitectonic characterization and functional decoding of four new areas in the human lateral orbitofrontal cortex [Original Research] *Frontiers in Neuroanatomy, 14*(2). https://doi.org/10.3389/fnana.2020.00002.

Wu, T., & Hallett, M. (2005). A functional MRI study of automatic movements in patients with Parkinson's disease. *Brain, 128*(10), 2250–2259. https://doi.org/10.1093/brain/awh569

Wu, T., & Hallett, M. (2013). The cerebellum in Parkinson's disease. *Brain, 136*(Pt 3), 696–709.

Yekutieli, D. (2008). Hierarchical false discovery rate–controlling methodology. *Journal of the American Statistical Association, 103*(481), 309–316. https://doi.org/10.1198/016214507000001373

Yushkevich, P. A., Piven, J., Hazlett, H. C., Smith, R. G., Ho, S., Gee, J. C., et al. (2006). User-guided 3D active contour segmentation of anatomical structures: Significantly improved efficiency and reliability. *NeuroImage, 31*(3), 1116–1128. https://doi.org/10.1016/j.neuroimage.2006.01.015

Zaborszky, L., Hoemke, L., Mohlberg, H., Schleicher, A., Amunts, K., & Zilles, K. (2008). Stereotaxic probabilistic maps of the magnocellular cell groups in human basal forebrain. *NeuroImage, 42*(3), 1127–1141. https://doi.org/10.1016/j.neuroimage.2008.05.055

Zachlod, D., Rüttgers, B., Bludau, S., Mohlberg, H., Langner, R., Zilles, K., et al. (2020). Four new cytoarchitectonic areas surrounding the primary and early auditory cortex in human brains. *Cortex, 128*, 1–21. https://doi.org/10.1016/j.cortex.2020.02.021

Zeighami, Y., Fereshtehnejad, S.-M., Dadar, M., Collins, D. L., Postuma, R. B., Mišić, B., et al. (2019). A clinical-anatomical signature of Parkinson's disease identified with partial least squares and magnetic resonance imaging. *NeuroImage, 190*, 69–78. https://doi.org/10.1016/j.neuroimage.2017.12.050

Zeighami, Y., Ulla, M., Iturria-Medina, Y., Dadar, M., Zhang, Y., Larcher, K. M.-H., et al. (2015). Network structure of brain atrophy in de novo Parkinson's disease. *eLife, 4*, Article e08440. https://doi.org/10.7554/eLife.08440